

# Petrogenesis of augite-bearing ureilites Hughes 009 and FRO 90054/93008 inferred from melt inclusions in olivine, augite and orthopyroxene

Cyrena Anne Goodrich<sup>a,\*</sup>, Anna Maria Fioretti<sup>b</sup>, James Van Orman<sup>c</sup>

<sup>a</sup> Department of Physical Sciences, Kingsborough Community College, 2001 Oriental Blvd., Brooklyn, NY 11235, USA

<sup>b</sup> CNR, Istituto di Geoscienze e Georisorse sezione di Padova, Corso Garibaldi 37, I-35127 Padova, Italy

<sup>c</sup> Department of Geological Sciences, Case Western Reserve University, Cleveland, OH 44120, USA

Received 7 July 2008; accepted in revised form 15 February 2009; available online 28 February 2009

## Abstract

Melt inclusions in ureilites occur only in the small augite- and orthopyroxene-bearing subgroups. Previously [Goodrich C.A., Fioretti A.M., Tribaudino M. and Molin G. (2001) Primary trapped melt inclusions in olivine in the olivine–augite–orthopyroxene ureilite Hughes 009. *Geochim. Cosmochim. Acta* **65**, 621–652] we described melt inclusions in olivine in the olivine–augite–orthopyroxene ureilite Hughes 009 (Hughes). FRO 90054/93008 (FRO) is a near-twin of Hughes, and has abundant melt inclusions in all three primary silicates. We use these inclusions to reconstruct the major, minor and rare earth element composition of the Hughes/FRO parent magma and evaluate models for the petrogenesis of augite-bearing ureilites.

Hughes and FRO consist of 23–47 vol % olivine (Fo 87.3 and 87.6, respectively), 7–52 vol % augite (*mg* 89.2, Wo 37.0 and *mg* 88.8, Wo 38.0, respectively), and 12–56 vol % orthopyroxene (*mg* 88.3, Wo 4.9 and *mg* 88.0, Wo 4.8, respectively). They have coarse-grained ( $\leq 3$  mm), highly-equilibrated textures, with poikilitic relationships indicating the crystallization sequence olivine → augite → orthopyroxene. FRO is more shocked than Hughes, experienced greater secondary reduction, and is more weathered. The two meteorites are probably derived from the same lithologic unit.

Melt inclusions in olivine consist of glass ± daughter cpx ± metal–sulfide–phosphide spherules ± chromite, and have completely reequilibrated Fe/Mg with their hosts. We follow the method of Goodrich et al. (2001) for reconstructing the composition of the primary trapped liquid they represent (olPTL), but correct an error in our treatment of the effects of reequilibration. Inclusions in augite consist of glass, which shows only partial reequilibration of Fe/Mg. The composition of the primary trapped liquid they represent (augPTL) is reconstructed by reverse fractional crystallization of wall augite from the most ferroan glass. Inclusions in orthopyroxene consist of glass + 30–50 vol % daughter cpx. The cpx shows complete, but the glass only partial, reequilibration of Fe/Mg. A range of possible compositions for the primary trapped liquid they represent (opxPTL) is calculated by modal recombination of glass and cpx, followed by addition of wall orthopyroxene and adjustment of Fe/Mg for equilibrium with the primary orthopyroxene. Only a small subset of these compositions is plausible on the basis of being orthopyroxene-saturated.

Results indicate that olPTL, assumed to represent the parent magma of these rocks, was saturated only with olivine and in equilibrium with Fo ~ 83. AugPTL and opxPTL are very similar in composition; both are close to augite + orthopyroxene co-saturation and in equilibrium with Fo 87/8. We suggest that olPTL was reduced to Fo 87/8 due to smelting during ascent, and show that this produces a composition very similar to that of augPTL and opxPTL.

REE data for each of the three primary silicates and the least evolved melt inclusions in olivine are used to calculate REE abundances in the Hughes/FRO parent magma. All four methods yield very similar results, indicating a REE pattern that is

\* Corresponding author. Present address: Planetary Science Institute, 1700 E. Ft. Lowell, Tucson, AZ 85719, USA.  
E-mail address: [cgoodrich@psi.edu](mailto:cgoodrich@psi.edu) (C.A. Goodrich).

strongly LREE-depleted ( $\text{Sm/La} = 3.3\text{--}3.7$ ), with a small negative Eu anomaly ( $\text{Eu/Eu}^* = 0.82$ ) and slight HREE-depletion ( $\text{Gd/Lu} = 1.4\text{--}1.6$ ).

The Hughes/FRO parent magma provides a robust constraint on models for the petrogenesis of augite-bearing ureilites. Its major, minor and rare earth element composition suggests derivation through mixing and/or assimilation processes, rather than as a primary melt on the ureilite parent body.

© 2009 Elsevier Ltd. All rights reserved.

## 1. INTRODUCTION

Main group ureilites are coarse-grained, highly-equilibrated ultramafic rocks characterized by high abundances of carbon, with metal, sulfide and phosphide as the only common accessory phases (Goodrich, 1992; Mittlefehldt et al., 1998). They can be subdivided (Goodrich et al., 2004, 2006) into three groups based on the identity of their pyroxenes: olivine–pigeonite, olivine–orthopyroxene and augite-bearing. Olivine–pigeonite ureilites (the most abundant) contain uninverted pigeonite ( $\text{Wo} \sim 6\text{--}13$ ) as their dominant pyroxene, and have Fo values ranging from  $\sim 76$  to 87 among samples. Olivine–orthopyroxene ureilites contain orthopyroxene ( $\text{Wo} \leq 5$ ) instead of, or in addition to, pigeonite, and have highly magnesian compositions ( $\text{Fo} \sim 86\text{--}92$ ). Together these two groups (the olivine–lpx ureilites) define a single Fe/Mg–Fe/Mn trend of near-constant, chondritic Mn/Mg (Fig. 1), which suggests that they are residues (consistent with their equilibrated textures) and are related to one another by various degrees of reduction

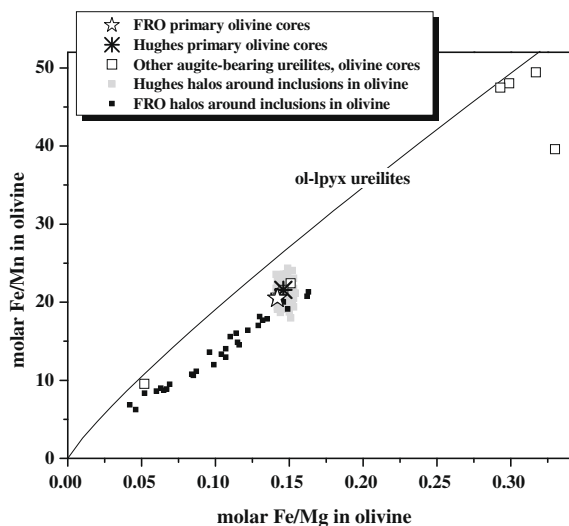


Fig. 1. Molar Fe/Mg vs. Fe/Mn of olivine in FRO and Hughes compared to other augite-bearing ureilites. Primary core compositions in Hughes and FRO, like those of the other augite-bearing ureilites, are offset from the trend defined by the olivine–low Ca pyroxene (ol–lpx) ureilites (Goodrich et al., 2006) as expected for fractionation of melts. Halos around melt inclusions in olivine in FRO show extensive secondary reduction, unlike those in Hughes. All data for primary core compositions are of high precision, with error bars on the order of the size of the symbols (Goodrich et al., 2001, 2006).

of common precursor material (Goodrich and Delaney, 2000). This reduction relationship among ureilites can be explained by smelting (carbon redox reactions) over a range of pressures on the ureilite parent body (Berkley and Jones, 1982; Goodrich et al., 1987, 2007; Warren and Kallemeyn, 1992; Walker and Grove, 1993; Sinha et al., 1997; Singletary and Grove, 2003), an interpretation that is supported by a correlation between Fo and pyroxene/olivine ratio and by the restriction of orthopyroxene to the most magnesian compositions. Based on the olivine–lpx ureilites, we have developed a model (Goodrich et al., 2007; Wilson et al., 2008) that encompasses petrologic, physical and thermal aspects of melting and smelting on an  $\sim 100$  km radius ureilite parent body (UPB).

In this paper, we address the origin of the relatively rare augite-bearing ureilites (8 out of 248 samples), which appear to be cumulates rather than residues (Goodrich et al., 2004, 2006). This interpretation is based largely on the Fe/Mg–Fe/Mn compositions of their olivine, which are displaced from the trend of the olivine–lpx ureilites (Fig. 1) as expected for fractionation of melts (Goodrich and Delaney, 2000). It is also suggested by the common occurrence of poikilitic textures, in which olivine and augite grains are enclosed in large (mm- to cm-sized) oikocrysts of low-Ca pyroxene and appear to have reacted with the melts from which their hosts crystallized (Goodrich, 1999a; Goodrich and Keller, 2000; Berkley and Goodrich, 2001).

In addition, several of the augite-bearing ureilites contain melt inclusions, which are not observed in the olivine–lpx ureilites. Goodrich et al. (2001) described abundant melt inclusions in olivine in Hughes 009, and reconstructed the composition of the primary trapped liquid (PTL) they represent. Subsequently, we discovered that FRO 90054 (paired with FRO 93008 and others as described below), a near-twin of Hughes 009, has abundant melt inclusions in olivine, augite and orthopyroxene. This prompted us to reexamine Hughes 009 and find melt inclusions (albeit scarce) in its augite and orthopyroxene as well. In this paper, we report petrographic and mineral compositional data for all primary minerals and melt inclusions in FRO 90054 (and paired samples), along with new data for melt inclusions in Hughes 009. In addition, we report rare earth element data for major phases and melt inclusions in both rocks. We then reconstruct the compositions of the PTLs represented by melt inclusions in olivine, augite and orthopyroxene (correcting an error in the reconstruction of Goodrich et al. (2001)), and use the results to examine the evolution of the Hughes/FRO parent magma during crystallization. Preliminary results of this work have been published in abstracts (Fioretti and Goodrich, 2000;

Goodrich and Fioretti, 2000, 2007; Goodrich et al., 2000; Goodrich, 2001). Finally, we use the composition of the Hughes/FRO parent magma to evaluate models for the petrogenesis of the augite-bearing ureilites.

## 2. ANALYTICAL METHODS

Electron microprobe analyses (EMPA) were conducted with the JEOL JXA 8900RL electron microprobe at Johannes Gutenberg Universität in Mainz, using methods described in Goodrich et al. (2001). The data presented for glasses in Hughes 009 represent new analyses since Goodrich et al. (2001). In that work, all glass analyses had low EMPA totals of ~96–98%, leading us to speculate that highly volatile species might be present. Subsequently, however, we discovered that although P was not evident in EDS spectra of the glasses (so that we omitted it from quantitative analyses), it was present in significant amounts (~1–3 wt% P<sub>2</sub>O<sub>5</sub>). In addition we found that although originally there appeared to be no evidence for loss of alkalis (Goodrich et al., 2001), new tests showed a small, but significant difference in Na<sub>2</sub>O contents between focused vs. defocused beam analyses. The new Hughes 009 glass analyses, including P<sub>2</sub>O<sub>5</sub> and using a defocused (5 µm) beam, have totals satisfactorily close to 100%. They do not differ significantly from those of Goodrich et al. (2001) for any elements other than Na<sub>2</sub>O, which shows slightly higher values. The data presented for glasses in FRO 90054 and FRO 93008 include analyses presented in abstract form in Fioretti and Goodrich (2000), in which P<sub>2</sub>O<sub>5</sub> was omitted, as well as later analyses that included P<sub>2</sub>O<sub>5</sub> and used a defocused beam. The two sets of analyses do not differ significantly (except for the omission of P<sub>2</sub>O<sub>5</sub> in the first set). Back-scattered electron images (BEI) were obtained using the JEOL JXA 8900RL microprobe in Mainz, and the JEOL 6390LV scanning electron microscope (SEM) in the Department of Physical Sciences at Kingsborough Community College.

Rare earth element (REE) analyses of Hughes 009 and FRO 90054 were made with the modified Cameca IMS3f ion microprobe at the Max Planck Institut für Chemie in Mainz, using a primary O-beam of 17 keV energy. The measurements were performed at low mass resolution ( $m/\Delta m = 500$ ) and with energy filtering of the secondary ion signal (~80 eV energy offset) to suppress contributions from molecular interferences to the elements of interest. Primary beam currents were ~10 or ~20 nA for the primary phases, and ~1 nA for phases in melt inclusions. In addition to REE, <sup>27</sup>Al and <sup>44</sup>Ca were monitored to ensure the identity of the material being analyzed. Data reduction followed the method of Zinner and Crozaz (1986), using Si as the reference element. Relative sensitivity factors were measured on NIST SRM 611 silicate glass (Rocholl et al., 1997) and on MPI DING glasses (Jochum et al., 2000). We also analyzed olivine in the olivine–pigeonite ureilite Kenna for comparison with the data of Guan and Crozaz (2000). The sections were examined by SEM after analysis, and in all but two cases (analyses of glasses that overlapped with surrounding olivine and were corrected for dilution) the analysis spot was found to be entirely within the phase of interest (e.g. Fig. 2f).

## 3. DESCRIPTION

### 3.1. Samples, general petrography and mineral compositions

Hughes 009 (hereafter, Hughes) has been described by Goodrich et al. (2001) and FRO 90054 by Baba et al. (1993), Tribaudino et al. (1997) and Fioretti and Goodrich (2000). FRO 93008 was considered by Fioretti and Molin (1996) and Fioretti and Goodrich (2000) to be paired with FRO 90054. However, Smith et al. (2000) described a section of FRO 93008 (,00) that consists of two distinct lithologies. Although one of these is, indeed, similar to FRO 90054, the other resembles typical olivine–pigeonite ureilites of Fo 78–79. The contact between these lithologies is brecciated and includes exotic material (Fioretti and Goodrich, 2001). Goodrich et al. (2004) suggested that FRO 93008 is a dimict breccia that was assembled in the aftermath of a catastrophic impact. Smith et al. (2000) pointed out that all (as of the time of that study) ureilites recovered from Frontier Mountain, Antarctica, consist of one of the two primary lithologies present in FRO 93008, and suggested that they were derived from a single meteoroid. Our concern here is only with the Fo 87 augite-bearing lithology in FRO 93008, which we find to be essentially identical to FRO 90054. We report observations from two thin sections of FRO 90054 (,07 and ,03), both sides of one thick section of FRO 90054 (,10 and ,10R), and three thin sections of FRO 93008 (,01 and ,02 in addition to ,00). We also studied one thin section of FRO 90228 that consists of the Fo ~ 87 augite-bearing lithology (Smith et al., 2000). Hereafter, we refer to all three samples of this lithology as FRO. We demonstrate below that Hughes and FRO are nearly twins but are not paired.

Both Hughes and FRO consist primarily of olivine, augite, and orthopyroxene (identified both compositionally and structurally), with minor metal, sulfide, and phosphide. They both have a coarse-grained (up to ~3 mm), highly-equilibrated texture (subhedral to euhedral grains and abundant 120° triple junctions) similar to that of typical olivine–pigeonite ureilites, and a slight preferential alignment of elongated grains. The observed range of modal abundances is: 23–47 vol % olivine, 7–52 vol % augite, and 12–56 vol % orthopyroxene (Baba et al., 1993; Fioretti and Molin, 1996; Tribaudino et al., 1997; Goodrich et al., 2001). In both samples, augite contains rounded chadocrysts of olivine, and orthopyroxene contains rounded chadocrysts of olivine and augite. Melt inclusions were not recognized in FRO in early studies (e.g. Baba et al., 1993; Tribaudino et al., 1997; Smith et al., 2000).

Olivine core compositions (Goodrich et al., 2001, 2006) show only subtle differences between samples: Fo 87.6 vs. 87.3, CaO = 0.281 ± 0.004 vs. 0.298 ± 0.006 wt% and Cr<sub>2</sub>O<sub>3</sub> = 0.541 ± 0.007 vs. 0.565 ± 0.013 wt% in FRO and Hughes, respectively. Fe–Mn–Mg compositions of olivine in both samples are displaced from the ureilite residue trend to higher Mn/Mg, as in all augite-bearing ureilites (Fig. 1). Augite and orthopyroxene compositions are also similar between the two samples, but in both cases differ significantly in Al<sub>2</sub>O<sub>3</sub> content (Table 1). Although both samples have very low abundances of carbon compared to other ureilites

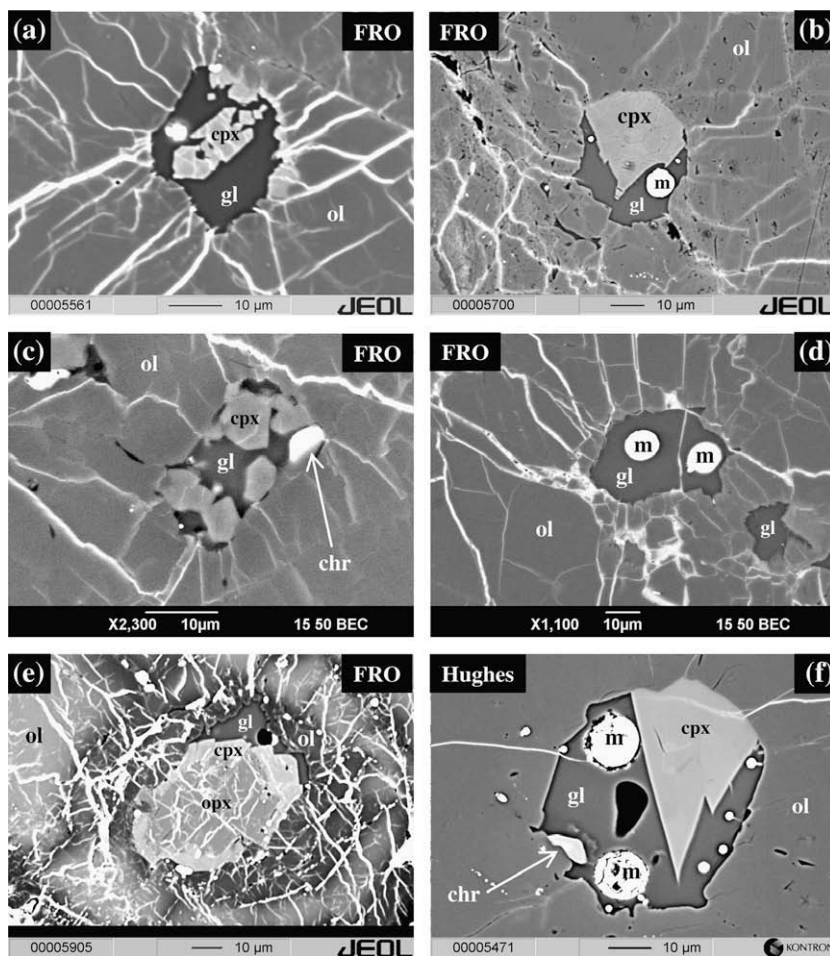


Fig. 2. Back-scattered electron images of melt inclusions in olivine (ol) in FRO and Hughes. Inclusions consist of glass (gl), daughter pyroxene (cpx), metal–phosphide–sulfide spherules (m) and rare chromite (chr). The unusual inclusion #24 shown in (e) contains a grain of orthopyroxene (opx) mantled by cpx, and is surrounded by an exceptionally large halo of secondary reduction. Hole in glass in (f) is ion microprobe pit, showing location of REE analysis. Samples: (a) FRO 90054,07; (b) FRO 93008,01; (c) FRO 90054,10R; (d) FRO 90054,03; (e) FRO 90054,10R; and (f) Hughes 009, B1.

(Grady and Pillinger, 1993; Smith et al., 1999; Goodrich et al., 2001), we observed one ~50- $\mu\text{m}$  sized, euhedral graphite crystal enclosed in olivine in FRO (section 90054,03). Both samples also show only a limited degree of secondary reduction of primary olivine compared to most ureilites. Both show only low to moderate, though highly heterogeneous, shock effects. FRO is significantly more weathered than Hughes: all sections show pervasive rust staining, and metallic phases are only rarely preserved.

### 3.2. Melt inclusions in olivine

Melt inclusion-bearing olivine crystals are more abundant in FRO than they are in Hughes. As in Hughes, those that do have inclusions generally have a large number of them, although none show the extreme concentration seen in Hughes (Goodrich et al., 2001). We counted more than 150 inclusions in at least 15 olivine crystals. They tend to cluster within their hosts, and commonly appear preferentially distributed along lines suggesting crystallographic

control. In terms of size (mostly 30–50  $\mu\text{m}$ , up to 130  $\mu\text{m}$ , in maximum dimension), morphology (boundaries with the host range from rounded or lobed to angular or subhedral), and phase assemblage (glass  $\pm$  Ca-rich pyroxene  $\pm$  spherules of metal, sulfide and phosphide,  $\pm$  minor grains of chromite) they are similar to inclusions in olivine in Hughes (Fig. 2). The Ca-rich pyroxene (cpx) occurs as partial rims (Fig. 2a) or sub/euhedral crystals protruding into the glass from the olivine (Fig. 2b and c), and/or as small, euhedral, skeletal or dendritic crystals that do not appear to be in contact with the olivine (Fig. 2a). The latter are more common than they are in inclusions in Hughes (Goodrich et al., 2001). Some inclusions have halos of surrounding olivine defined by small grains of metal and/or thin, discontinuous arcs of glass, similar to those in Hughes (Goodrich et al., 2001) but less pronounced. In addition, in most cases the immediately surrounding olivine shows irregular belts or patches of secondary reduction (up to Fo 96), which were not observed in Hughes. Furthermore, almost all inclusions are surrounded by subradial cracks

Table 1  
Compositions of primary pyroxenes in FRO and Hughes (oxides in wt%).

	Augite		Orthopyroxene	
	FRO avg. (31)	Hughes <sup>a</sup> avg. (98)	FRO avg. (41)	Hughes <sup>a</sup> avg. (113)
SiO <sub>2</sub>	53.4 ± 0.4	53.7 ± 0.5	55.8 ± 0.3	55.9 ± 0.4
TiO <sub>2</sub>	0.23 ± 0.04	0.27 ± 0.05	0.11 ± 0.04	0.13 ± 0.02
Al <sub>2</sub> O <sub>3</sub>	1.93 ± 0.06	1.61 ± 0.12	1.21 ± 0.02	1.01 ± 0.02
Cr <sub>2</sub> O <sub>3</sub>	1.33 ± 0.03	1.29 ± 0.05	1.06 ± 0.02	1.04 ± 0.04
FeO	4.34 ± 0.49	4.30 ± 0.20	7.48 ± 0.31	7.30 ± 0.20
MgO	19.3 ± 0.2	19.7 ± 0.3	30.7 ± 0.2	31.1 ± 0.3
MnO	0.42 ± 0.04	0.41 ± 0.02	0.55 ± 0.04	0.54 ± 0.02
CaO	18.5 ± 0.2	18.1 ± 0.3	2.47 ± 0.04	2.51 ± 0.03
Na <sub>2</sub> O	0.24 ± 0.02	0.27 ± 0.02	0.04 ± 0.02	0.05 ± 0.01
Total	99.7	99.7	99.4	99.6
<i>mg</i> <sup>b</sup>	88.8 ± 1.2	89.2 ± 0.4	88.0 ± 0.5	88.3 ± 0.2
Fe/Mg <sup>c</sup>	0.126 ± 0.015	0.121 ± 0.004	0.137 ± 0.006	0.132 ± 0.003
Wo <sup>d</sup>	38.0 ± 0.4	37.0 ± 0.7	4.8 ± 0.1	4.9 ± 0.1

<sup>a</sup> Goodrich et al. (2001).

<sup>b</sup> In all tables *mg* = molar MgO/(MgO + FeO).

<sup>c</sup> In all tables Fe/Mg = molar FeO/MgO.

<sup>d</sup> In all tables Wo = molar CaO/(CaO + FeO + MgO).

(generally filled with iron oxides), a feature not observed in Hughes.

One unusual inclusion (#24) in olivine contains a 20–25- $\mu$ m sized grain of orthopyroxene that is almost completely mantled by cpx (Fig. 2e). The orthopyroxene has a subhedral shape, which is mimicked by the cpx mantle but with prominent embayments that give it the appearance of having been resorbed (Fig. 2e). Orthopyroxene has not been observed in any other inclusion in FRO. In Hughes it was found in only one inclusion – as small (~2–3  $\mu$ m) tips on cpx crystals (Goodrich et al., 2001). Inclusion #24 has an exceptionally large halo of secondary reduction.

Compositions of glasses and cpx from ~100 inclusions in olivine in FRO are shown in Figs. 3 and 4, compared with those in Hughes. Selected analyses are given in Table 2. Glasses have Al<sub>2</sub>O<sub>3</sub> contents of 17.5–26.4 wt%. They show continuous compositional trends with negative correlations of CaO, TiO<sub>2</sub> and Cr<sub>2</sub>O<sub>3</sub>, and positive correlations of SiO<sub>2</sub> and Na<sub>2</sub>O with Al<sub>2</sub>O<sub>3</sub>, very similar to those shown by glasses in Hughes but slightly shifted towards higher Al<sub>2</sub>O<sub>3</sub> (Figs. 3 and 4). Fe/Mg values, as in Hughes, show no correlation with Al<sub>2</sub>O<sub>3</sub>; the majority of analyses cluster near the same value as in Hughes (0.61) but show greater scatter. In addition, Fe/Mg, Na<sub>2</sub>O and SiO<sub>2</sub> all show nearly vertical sub-trends at ~22 wt% Al<sub>2</sub>O<sub>3</sub> (Figs. 3 and 4). P<sub>2</sub>O<sub>5</sub> shows a weak negative correlation with Al<sub>2</sub>O<sub>3</sub> in both Hughes and FRO (Fig. 4).

Cpx both within and among inclusions in FRO shows compositional trends nearly identical to those of cpx in inclusions in Hughes: CaO, TiO<sub>2</sub> and Na<sub>2</sub>O increase, while Cr<sub>2</sub>O<sub>3</sub> increases and then decreases (though with considerable scatter) with increasing Al<sub>2</sub>O<sub>3</sub> (Fig. 3). As in Hughes, these trends begin near the composition of the primary augite but extend to very high values. Fe/Mg values show much less variation (0.15 ± 0.05), and are only slightly higher than that of the primary augite (0.126).

In Hughes, we documented zoning of CaO and Cr<sub>2</sub>O<sub>3</sub> in olivine halos surrounding the inclusions (Goodrich et al., 2001). We were unable to do so in FRO because of the high abundance of cracks. However, spot analyses within ~15  $\mu$ m of the inclusions show lower CaO and Cr<sub>2</sub>O<sub>3</sub> relative to the primary olivine, to nearly the same degree as in Hughes. In Hughes the halo olivine shows nearly constant Fe/Mg identical to that of the primary olivine; in contrast, in FRO, it is strongly reduced (Fig. 1).

In the unusual inclusion #24, the orthopyroxene core is homogeneous and similar in composition to the primary orthopyroxene. The cpx mantle is heterogeneous and follows the same compositional trends as daughter cpx in other inclusions (Al<sub>2</sub>O<sub>3</sub> = 2.4–5.9 wt%). The glass is also within the compositional range of glasses from other inclusions (Al<sub>2</sub>O<sub>3</sub> = 23–24 wt%). Both the cpx and the glass, however, are significantly more reduced than in other inclusions.

### 3.3. Melt inclusions in augite

Melt inclusions in augite are much less abundant than those in olivine. We observed 14 (in 7 host crystals) in FRO and 2 in Hughes. They are  $\leq$ 30  $\mu$ m in maximum dimension and irregular in shape (Fig. 5a and b). They contain no daughter silicates and only rare metal–sulfide spherules. They are typically surrounded by radial cracks filled with iron oxides (Fig. 5a and b).

Glasses in these inclusions show a restricted range of Al<sub>2</sub>O<sub>3</sub> content (20.7–23.4 wt%), and plot along the trends defined by glasses in inclusions in olivine for Al<sub>2</sub>O<sub>3</sub> vs. CaO, Cr<sub>2</sub>O<sub>3</sub> and (with the exception of one group of analyses) TiO<sub>2</sub> (Fig. 3 and Table 3). Na<sub>2</sub>O contents form an essentially vertical trend, coincident with the subtrend noted for Na<sub>2</sub>O in glasses in olivine at ~22 wt% Al<sub>2</sub>O<sub>3</sub>. SiO<sub>2</sub> contents are all significantly lower (by ~5 wt% on

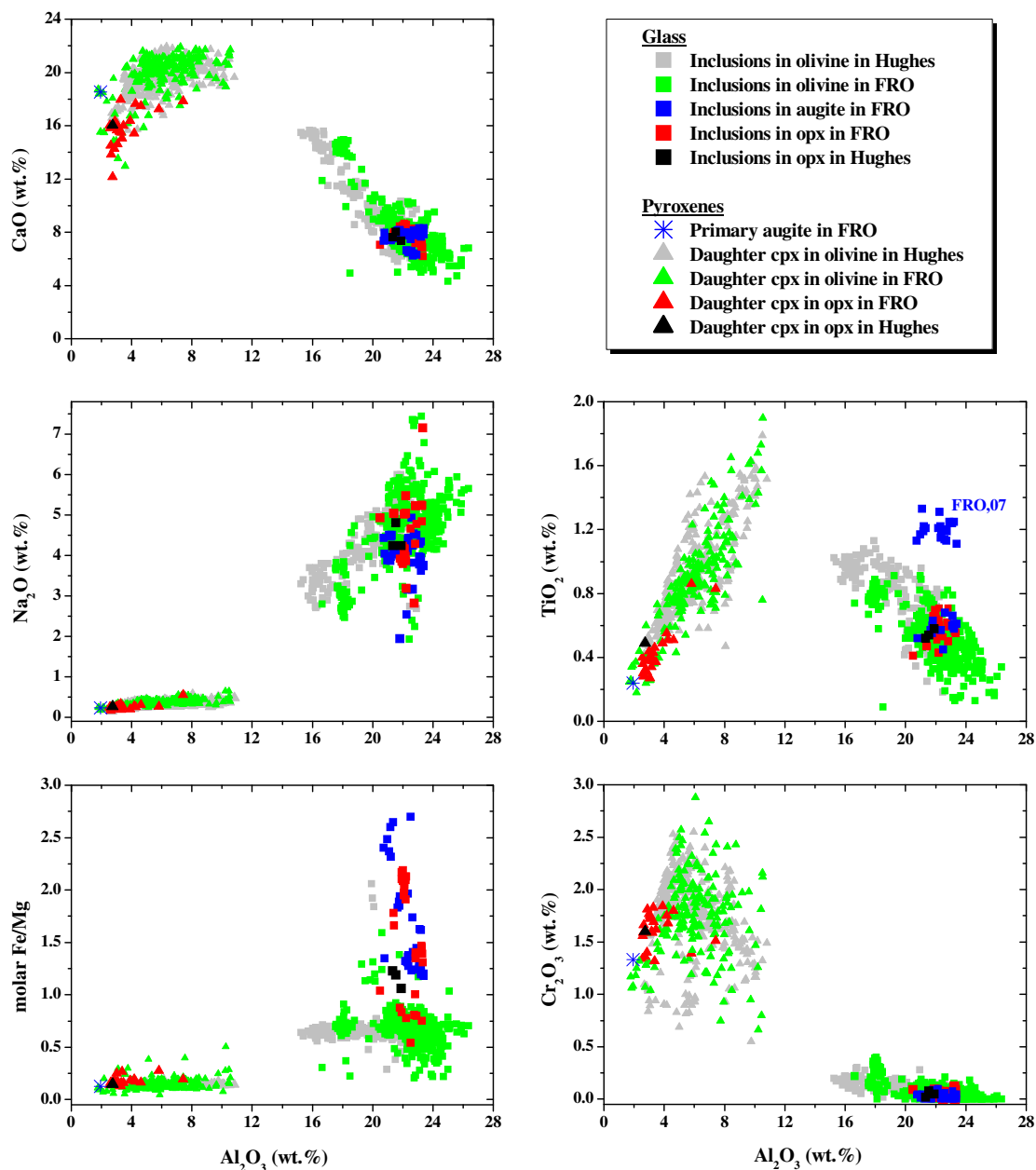


Fig. 3.  $\text{Al}_2\text{O}_3$  vs.  $\text{CaO}$ ,  $\text{Na}_2\text{O}$ ,  $\text{TiO}_2$ ,  $\text{Cr}_2\text{O}_3$  (all wt%) and molar  $\text{Fe}/\text{Mg}$  for glasses and daughter pyroxene (cpx) in melt inclusions in olivine, augite, and orthopyroxene (opx) in Hughes and FRO. Primary augite in FRO also shown for reference. Group of outlying analyses of glasses in inclusions in augite labeled FRO ,07 on  $\text{TiO}_2$  plot are all from section FRO 90054,07. Data for cpx in inclusions in olivine in Hughes from Goodrich et al. (2001).

average) and  $\text{P}_2\text{O}_5$  contents higher than those of glasses in inclusions in olivine at the same  $\text{Al}_2\text{O}_3$  contents (Fig. 4). In addition, their  $\text{Fe}/\text{Mg}$  ratios (Fig. 3) are higher and much more variable (1.2–2.7). The group of analyses with exceptional (high)  $\text{TiO}_2$  contents are all from section FRO 90054,07 (3 inclusions), and show anomalously high  $\text{K}_2\text{O}$  (up to 1.2 wt%) as well (Table 3).

Halo augite (within a distance of  $\sim 10 \mu\text{m}$  from the inclusions) is slightly depleted in  $\text{Cr}_2\text{O}_3$  and  $\text{CaO}$  relative to the primary augite (Table 3). Halo augite in FRO 90054,07 shows anomalously low  $\text{Al}_2\text{O}_3$  and high  $\text{TiO}_2$  compared to other sections (Table 3).

### 3.4. Melt inclusions in orthopyroxene

Melt inclusions in orthopyroxene are also much less abundant than those in olivine. We observed 10 in FRO (in 6 host crystals) and 2 in Hughes. They are  $\leq 40 \mu\text{m}$  in maximum dimension and typically show subhedral (i.e. negative crystal) to irregular shapes (Fig. 5c and d). In some cases they show halos defined by tiny grains of metal and glass. They consist of glass and cpx  $\pm$  metal–sulfide–phosphide spherules. The cpx occurs as subhedral crystals in contact with the surrounding orthopyroxene. Compositionally, the glasses in these inclusions are similar to those of

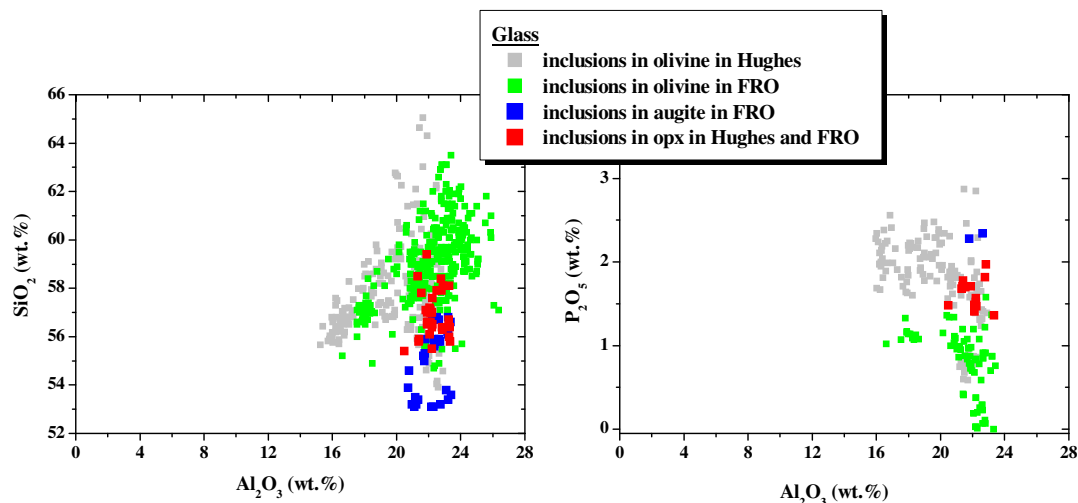


Fig. 4.  $\text{Al}_2\text{O}_3$  vs.  $\text{SiO}_2$  and  $\text{P}_2\text{O}_5$  (all wt%) in glasses in melt inclusions in olivine, augite, and orthopyroxene in Hughes and FRO.

inclusions in augite, with the exception that their  $\text{SiO}_2$  contents are slightly higher (Figs. 3 and 4; Table 4). The cpx plots along the trends defined by cpx in inclusions in olivine, with a restricted range of low- $\text{Al}_2\text{O}_3$  compositions (Figs. 3 and 4; Table 4). As for cpx in inclusions in olivine, Fe/Mg ratios are quite homogeneous ( $0.17 \pm 0.04$ ) and only slightly higher than that of the primary orthopyroxene (0.137). Compositions of opx in the halos are similar to that of the primary opx.

### 3.5. Rare earth elements

Rare earth element data are given in electronic annex EA-1 (Hughes) and EA-2 (FRO), and are shown on CI-normalized abundance plots in Fig. 6. All the olivines have very low REE abundances and strongly LREE-depleted

patterns with values for La to Eu being below the detection limit of  $\sim 1$  ppb (Fig. 6a). Results for Kenna ( $\text{Yb} = 0.28 \times \text{CI}$ ,  $\text{Gd} = 0.005 \times \text{CI}$ ) are within error identical to those of Guan and Crozaz (2000). Compared to Kenna, olivines in Hughes and FRO have somewhat higher REE abundances ( $\text{Yb}$  up to  $0.53 \times \text{CI}$ ) and shallower slopes ( $\text{Gd} = 0.03\text{--}0.05 \times \text{CI}$ ). The primary orthopyroxenes (Fig. 6a) also have overall LREE-depleted patterns ( $\text{Lu} = 1.1\text{--}2.4 \times \text{CI}$  and La generally  $0.005\text{--}0.01 \times \text{CI}$ ), with large negative Eu anomalies ( $\text{Eu}/\text{Eu}^* = 0.08\text{--}0.42$ ). One of the FRO analyses shows higher LREE and a shallower pattern, but this could be due to LREE contamination during weathering. The primary augites (Fig. 6a) show nearly flat HREE (Gd to Lu) patterns at  $\sim 3\text{--}5 \times \text{CI}$ , but are LREE-depleted with  $\text{La} = 0.14\text{--}0.17 \times \text{CI}$  (except, again, one FRO analysis that may reflect contam-

Table 2

Compositions of glass and daughter cpx in melt inclusions in olivine in FRO and Hughes (oxides in wt%).

	Hughes <sup>a</sup>		FRO				
	Glass		Glass			Cpx	
	Low-Al	High-Al	Low-Al	High-Al	High-Al	Low-Al	High-Al
$\text{SiO}_2$	56.8	59.0	57.3	59.2	60.1	54.3	46.6
$\text{TiO}_2$	1.03	0.56	0.82	0.42	0.18	0.35	1.73
$\text{Al}_2\text{O}_3$	16.0	22.5	17.8	22.6	25.9	2.0	10.5
$\text{Cr}_2\text{O}_3$	0.22	0.06	0.18	0.08	0.00	1.08	1.81
$\text{FeO}$	2.82	2.24	2.74	2.10	1.64	3.77	4.10
$\text{MgO}$	2.55	1.85	2.19	2.16	1.30	22.2	14.1
$\text{MnO}$	0.19	0.21	0.19	0.23	0.13	0.54	0.43
$\text{CaO}$	15.1	7.3	14.0	8.4	5.9	15.5	20.6
$\text{K}_2\text{O}$	0.03	0.09	0.07	0.04	0.06	na	na
$\text{Na}_2\text{O}$	3.19	5.64	3.72	4.88	5.28	0.17	0.44
$\text{P}_2\text{O}_5$	2.28	1.24	1.33	0.25	na <sup>b</sup>	na	na
Total	100.2	100.7	100.3	100.4	100.5	99.9	100.3
<i>mg</i>	61.7	59.6	58.8	64.7	58.5	91.3	86.0
Fe/Mg	0.620	0.679	0.702	0.545	0.710	0.095	0.163
Wo						31.5	47.4

<sup>a</sup> Reanalyzed after Goodrich et al. (2001), with defocused beam and including  $\text{P}_2\text{O}_5$ .

<sup>b</sup> In all tables, na = not analyzed.

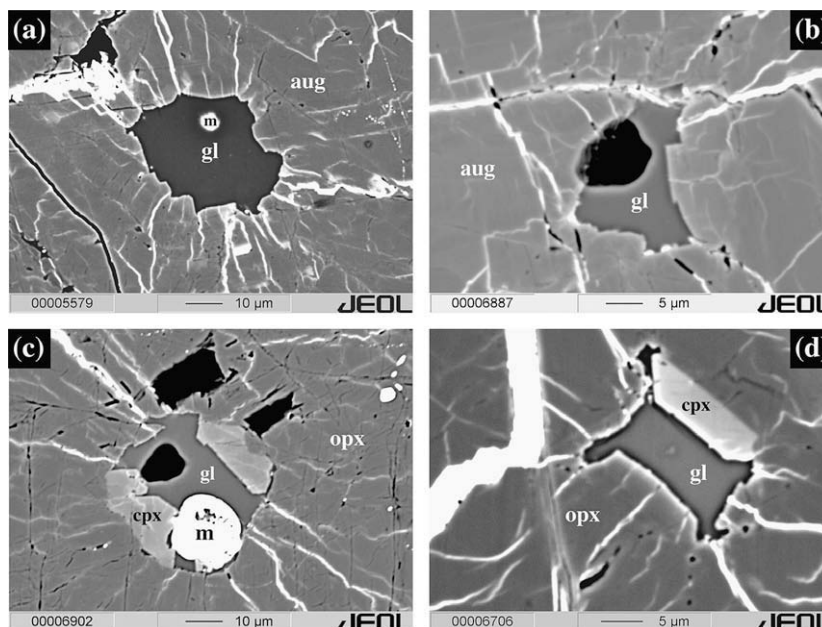


Fig. 5. Back-scattered electron images of melt inclusions in augite and orthopyroxene in FRO. (a) Melt inclusion in augite (aug) consisting of glass (gl) and metal-phosphide-sulfide spherule (m). (b) Melt inclusion in augite consisting of glass. (c) Melt inclusion in orthopyroxene (opx) consisting of glass, daughter pyroxene (cpx) and metal-phosphide-sulfide spherule. (d) Melt inclusion in orthopyroxene consisting of glass and daughter cpx. Holes in glass in (b) and (c) are ion microprobe pits, showing locations of rare earth element analyses. Samples: (a) FRO 90054,07; (b) FRO 90054,10; (c and d) FRO 90054,10R.

ination) and small negative Eu anomalies ( $\text{Eu}/\text{Eu}^* = 0.30\text{--}0.68$ ). Except for possible effects of contamination, there are no significant differences in REE abundances of the primary phases between Hughes and FRO.

High-Ca pyroxenes in the inclusions in olivine have REE patterns that are very similar to those of the primary augite, but at higher abundance levels and with larger Eu anomalies (Fig. 6a and b): Gd to Lu  $\sim 14\text{--}29 \times \text{CI}$ , La = 0.7–1.6,  $\text{Eu}/\text{Eu}^* = 0.13\text{--}0.26$ . The glasses have pat-

terns that, from Pr to Lu, are either essentially flat or slightly HREE-depleted at  $\sim 10\text{--}30 \times \text{CI}$ , and generally show a small, positive Eu anomaly; from La to Pr they show LREE-depleted patterns, with La  $\sim 5\text{--}11 \times \text{CI}$ . Glasses in inclusions in augite and orthopyroxene in FRO have REE patterns and abundances that are quite similar to those of inclusions in olivine (Fig. 6c), with the exception that the glasses in orthopyroxene show larger Eu anomalies ( $\text{Eu}/\text{Eu}^* = 2.7$ ).

Table 3

Compositions of glass and halo augite in melt inclusions in augite in FRO (oxides in wt%).

	Most ferroan glass	FRO ,07 glass	avg. (12) <sup>b</sup> glass	Most ferroan avg. glass <sup>c</sup>	avg. (46) <sup>a</sup> halo augite	FRO ,07 halo augite
SiO <sub>2</sub>	56.8	56.8	56.0 ± 0.7	55.4	53.4 ± 0.5	54.1
TiO <sub>2</sub>	0.45	1.31	0.59 ± 0.06	0.58	0.24 ± 0.05	0.46
Al <sub>2</sub> O <sub>3</sub>	22.5	22.2	22.5 ± 0.8	22.2	2.06 ± 0.34	1.55
Cr <sub>2</sub> O <sub>3</sub>	0.03	0.05	0.04 ± 0.03	0.04	1.29 ± 0.05	1.28
FeO	5.45	4.58	5.00 ± 0.57	6.15	4.69 ± 0.75	3.90
MgO	1.13	1.95	1.74 ± 0.29	1.1	19.4 ± 0.4	19.8
MnO	0.29	0.43	0.32 ± 0.04	0.32	0.41 ± 0.03	0.40
CaO	7.48	6.65	7.98 ± 0.25	7.9	18.3 ± 0.4	18.9
K <sub>2</sub> O	0.05	1.21	0.08 ± 0.03	0.08	na	na
Na <sub>2</sub> O	4.24	2.54	4.00 ± 0.29	3.96	0.25 ± 0.05	0.25
P <sub>2</sub> O <sub>5</sub>	na	na	2.31	2.29	na	na
Total	98.4	97.7	100.6	100	100.0	100.6
mg	27.0	43.1	38.2 ± 5.5	24.3	88.0 ± 1.8	90.1
Fe/Mg	2.7 <sup>a</sup>	1.32	1.62 ± 0.41	3.1	0.136 ± 0.024	0.110
Wo					37.3 ± 0.7	38.2

<sup>a</sup> Analytical uncertainty ±0.4.

<sup>b</sup> Excluding section FRO 90054,07 (FRO ,07). For glass, P<sub>2</sub>O<sub>5</sub> = average of two values only.

<sup>c</sup> Average glass with Fe/Mg adjusted to the upper limit of the most ferroan glass.

Table 4  
Compositions of glass and pyroxenes in melt inclusions in orthopyroxene (opx) in FRO and Hughes (oxides in wt%).

	Most ferroan glass	avg. (31) glass 1 <sup>b</sup>	avg. (22) glass 2 <sup>c</sup>	Most ferroan avg. glass 1 <sup>d</sup>	Most ferroan avg. glass 2 <sup>e</sup>	avg. (22) daughter cpx	avg. (107) halo opx
SiO <sub>2</sub>	56.6	56.8 ± 0.8	57.2 ± 0.7	57.1	56.7	52.2 ± 1.3	56.0 ± 0.4
TiO <sub>2</sub>	0.67	0.58 ± 0.08	0.61 ± 0.06	0.60	0.58	0.43 ± 0.15	0.11 ± 0.03
Al <sub>2</sub> O <sub>3</sub>	22.0	22.3 ± 0.6	22.2 ± 0.4	22.2	22.2	3.55 ± 1.17	1.24 ± 0.10
Cr <sub>2</sub> O <sub>3</sub>	0.06	0.05 ± 0.03	0.05 ± 0.02	0.05	0.05	1.62 ± 0.17	1.05 ± 0.04
FeO	4.91	4.15 ± 0.98	3.94 ± 0.88	4.80	5.03	6.11 ± 1.2	7.59 ± 0.43
MgO	1.26	1.64 ± 0.51	1.57 ± 0.45	1.08	1.13	19.9 ± 1.6	30.9 ± 0.4
MnO	0.25	0.30 ± 0.05	0.29 ± 0.04	0.28	0.30	0.57 ± 0.05	0.56 ± 0.03
CaO	8.25	7.90 ± 0.60	8.20 ± 0.30	8.18	7.87	15.8 ± 1.41	2.49 ± 0.10
K <sub>2</sub> O	0.08	0.06 ± 0.02	0.06 ± 0.02	0.06	0.06	na	na
Na <sub>2</sub> O	3.79	4.52 ± 0.81	4.13 ± 0.54	4.13	4.51	0.26 ± 0.08	0.04 ± 0.02
P <sub>2</sub> O <sub>5</sub>	na	1.61 ± 0.19	1.58 ± 0.15	1.57	1.60	na	na
Total	97.9	99.9	99.8	100.0	100.0	100.4	100.0
mg	31.4	41.3 ± 10.0	41.5 ± 11.7	28.6	28.6	85.3 ± 11.7	87.9 ± 0.7
Fe/Mg	2.19 <sup>a</sup>	1.42 ± 0.55	1.41 ± 0.64	2.49	2.49	0.172 ± 0.64	0.138 ± 0.009
Wo						32.8 ± 3.5	4.84 ± 0.20

<sup>a</sup> Analytical uncertainty ±0.3.

<sup>b</sup> Average of all glass analyses (P<sub>2</sub>O<sub>5</sub> from only 11).

<sup>c</sup> Average of major trend of analyses, 7 out of 9 inclusions (P<sub>2</sub>O<sub>5</sub> from only 6).

<sup>d</sup> Average glass 1 with Fe/Mg adjusted to upper limit of the most ferroan glass.

<sup>e</sup> Average glass 2 with Fe/Mg adjusted to upper limit of the most ferroan glass.

The analyzed glasses from inclusions in olivine cover nearly the full range of observed glass compositions (Fig. 3), with Al<sub>2</sub>O<sub>3</sub> contents of ~17–23 wt% (Fig. 6d). There appears to be a positive correlation between LREE (La to Nd) abundances and Al<sub>2</sub>O<sub>3</sub> content among the glasses (Fig. 6d). The analyzed cpx were all zoned, but due to constraints of crystal size and the necessity of avoiding cracks, it turned out that the areas analyzed in each had similar compositions (Wo ~ 42, Al<sub>2</sub>O<sub>3</sub> = 4.6 wt%).

#### 4. DISCUSSION

In terms of primary petrographic features, Hughes and FRO are virtually identical, except for slight differences in the compositions of their primary pyroxenes (Table 1). In terms of secondary features they differ more. FRO appears to be more shocked and has experienced a greater degree of secondary reduction, which may reflect differences in excavation and/or reassembly history (e.g. Goodrich et al., 2004). FRO is also significantly more weathered. These secondary effects do not obscure their primary similarity, and it is likely that these two ureilites are derived from the same lithologic unit on the UPB.

Poikilitic relationships observed in Hughes and FRO suggest the crystallization sequence olivine → augite → orthopyroxene, as inferred for other augite-bearing ureilites (Goodrich et al., 2004, 2006). The occurrence of melt inclusions in all three of these phases thus presents a rare opportunity to track the evolution of a ureilitic melt during crystallization, and obtain information about chemical and physical conditions of formation that can be used to constrain models for the petrogenesis of augite-bearing ureilites.

Unfortunately, retrieving the composition of the primary trapped liquid (PTL) represented by a set of melt

inclusions is usually not trivial. Trapped melts invariably fractionate during cooling, at least through continuing crystallization of the host phase (with which they must be saturated) onto inclusion walls (Roedder, 1976, 1979; Sobolev, 1996) and often through crystallization of daughter minerals as well. Furthermore, they may experience chemical exchange reactions with their hosts, most commonly Fe–Mg reequilibration (Sobolev, 1996; Danyushevsky et al., 2000, 2002a; Gaetani and Watson, 2000).

Methodologies for reversing these effects through experimental rehomogenization are well established (Sobolev, 1996; Danyushevsky et al., 2002a,b). However, methodologies for doing so analytically (often the only option in the case of rare materials such as meteorites) have not been standardized. Generally, each set of inclusions presents unique challenges, and it requires detailed study to reveal all post-entrapment modifications, devise techniques for reversing them, and realistically estimate the uncertainties involved in doing so. Although it is true that results cannot always be tested against independent information, in the case of Hughes/FRO at least one test would be whether the three melt compositions present a sensible picture of magmatic evolution. Thus, in the following sections, we independently reconstruct primary trapped liquid compositions for each of the three host minerals.

##### 4.1. Melt inclusions in olivine

Goodrich et al. (2001) reconstructed the composition of the PTL represented by melt inclusions in olivine in Hughes. We showed that this set of inclusions presents a fortuitous case in which reintegration of daughter crystals with residual liquid (glass) does not require modal recombination or broad beam analysis techniques, either of which can introduce significant uncertainties (e.g. Treiman,

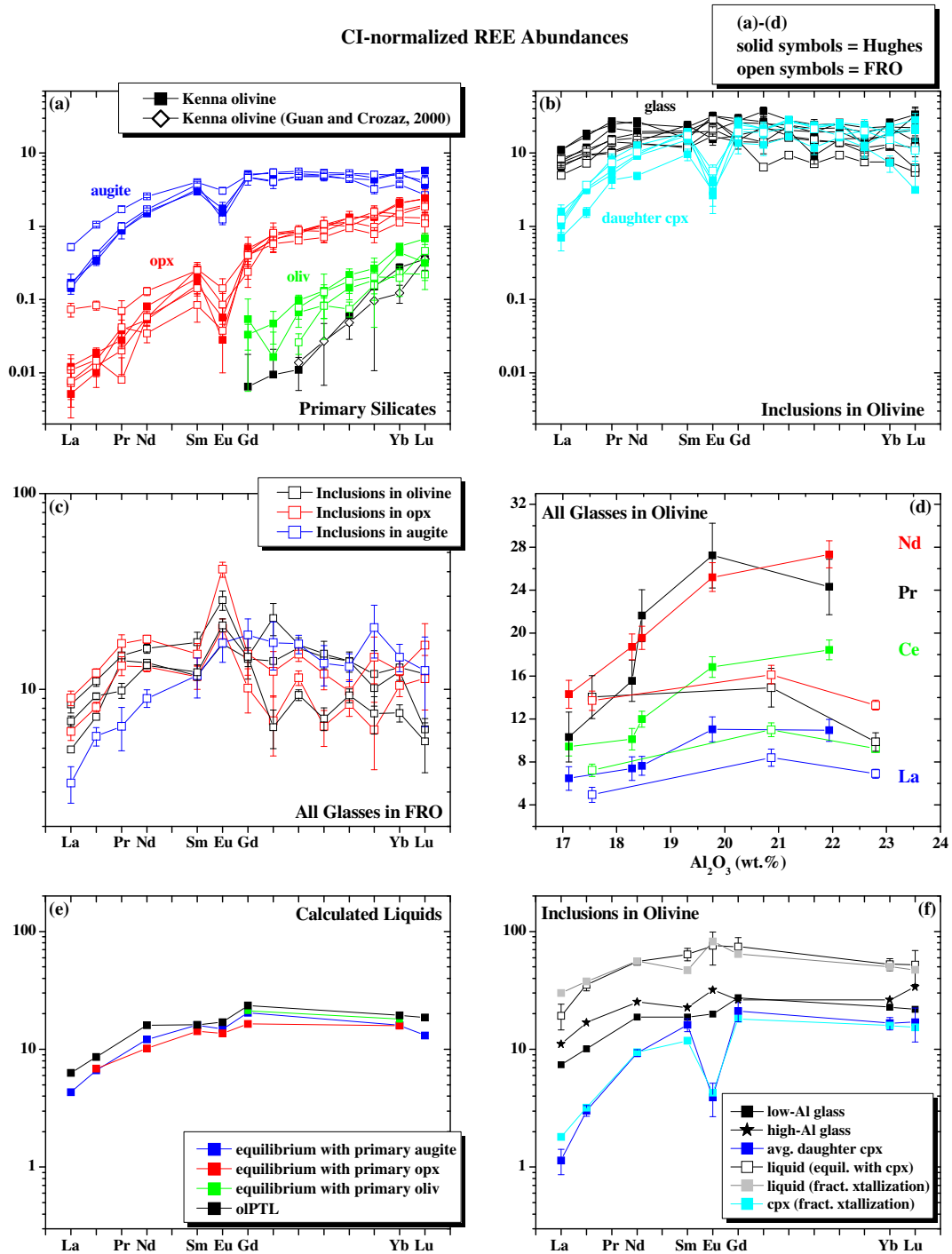


Fig. 6. CI-normalized rare earth element (REE) abundances. (a) Primary silicates in Hughes and FRO, and olivine in the olivine–pigeonite ureilite Kenna. (b) Glasses and daughter pyroxene (cpx) in inclusions in olivine in Hughes and FRO. (c) Glasses in inclusions in olivine, augite and orthopyroxene in FRO. (d) Light rare earth elements vs.  $Al_2O_3$  content of glasses in olivine in Hughes and FRO. (e) REE abundances of liquids calculated to be in equilibrium with the primary olivine, augite and orthopyroxene in Hughes/FRO, and of the primary trapped liquid represented by melt inclusions in olivine (oIPTL) calculated from the low- $Al_2O_3$  glass. (f) REE abundances of liquid calculated to be in equilibrium with the average daughter cpx in inclusions in olivine in Hughes and FRO, and of liquid plus cpx calculated as products of 30–50% fractional crystallization from the low- $Al_2O_3$  glass. Distribution coefficients used for calculations given in Table 6. CI abundances from Anders and Ebihara (1982).

1993; Ikeda, 1998). This arises because the compositional trends of the glasses in the inclusions (for all elements ex-

cept Fe and Mg) can be demonstrated to result principally from various degrees of crystallization of the observed cpx,

the only major daughter phase (Goodrich et al., 2001). Thus, it requires only a small extrapolation from the composition of the least aluminous glass (LAG) to arrive at the composition of the melt before any pyroxene crystallized (ur-LAG). We have no reason to doubt that the major part of that reconstruction is robust (we have revised the ur-LAG based on new analyses, but it does not differ significantly from the old one: Table 5), nor that it pertains equally to the inclusions in olivine in FRO. Our detailed observations of the FRO inclusions show that in terms of all primary features they are essentially identical to the Hughes inclusions. Small differences such as the slight shift of glass compositions to higher  $\text{Al}_2\text{O}_3$  and more common occurrence of skeletal morphology in daughter cpx in FRO can be explained by slight differences in nucleation rate within the inclusions (e.g. Frezzotti, 2001). We have, however, discovered a significant error in our treatment of Fe/Mg reequilibration in the inclusions, and here we rectify it.

The Hughes inclusions show clear evidence of Fe/Mg reequilibration with their hosts: halo olivine is homogeneous and identical in Fe/Mg to the host, pyroxenes are likewise homogeneous and nearly identical to the primary augite (Fig. 3), and glasses are nearly homogeneous  $mg \sim 62$  (Fig. 3). The FRO inclusions show the same effects, although their halos have been disturbed by late reduction. Furthermore, Goodrich et al. (2001) noticed that although the compositional trends of the glasses could be explained by crystallization of the observed cpx, in the Ol–Qtz–Wo system the glasses show a trend that is significantly offset relative to that expected from crystallization of the pyroxene (Fig. 7a). We interpreted this offset to be due to “Fe-loss” (Danyushevsky et al., 2000) during reequilibration, and showed that it could be “reversed” by addition

of  $\sim 10$  mol % FeO. Adding 10 mol % FeO to the ur-LAG produced a composition which we understood to be that of the residual liquid in the inclusions after fractional crystallization of wall olivine, so that a reverse fractional crystallization calculation (Sobolev and Shimizu, 1993) could be used to reintegrate the wall olivine and restore the PTL. However, this interpretation was incorrect. The following discussion is intended to clarify the “Fe-loss” effect (Danyushevsky et al., 2000), which has not been widely recognized or properly understood in analytical studies of melt inclusions.

Reequilibration of olivine-hosted melt inclusions occurs in all but the most rapidly cooled cases, due to high rates of coupled Fe–Mg diffusion in olivine (Danyushevsky et al., 2000, 2002a). During reequilibration, the fractionally crystallized wall olivine loses FeO and gains MgO through exchange with the surrounding host (Figs. 8 and 9). Because diffusion in melts is at least as fast as it is in olivine, the residual liquid in the inclusions will also reequilibrate, by losing FeO and gaining MgO to maintain equilibrium with the olivine (Fig. 8b). However, an important effect that is not widely recognized is that the flux of MgO into the liquid causes it to become supersaturated with olivine, leading to crystallization of “excess” olivine relative to the case of no reequilibration. This leaves the residual liquid severely depleted not only in the FeO that is lost to the host, but also in MgO that is sequestered in the excess olivine (Figs. 8b and 9c). Thus, although the glass will have a high  $mg$  ratio reflecting equilibrium with the surrounding host, this is potentially misleading (in the worst case, this liquid can be mistaken for the unmodified PTL) because absolute concentrations of FeO and MgO are extremely low (Fig. 9c).

The use of the term “Fe-loss” to describe this effect (misinterpreted to mean that FeO can be lost or gained indepen-

Table 5  
Reconstructed compositions for melt inclusions in Hughes and FRO (oxides in wt%).

	G01 <sup>a</sup> ur-LAG 1	ur-LAG	G01 <sup>a</sup> PLT1	olPTL <sup>b</sup>	olPTL-R <sup>c</sup>	augPTL2 <sup>d</sup>	opxPTL <sup>e</sup>
SiO <sub>2</sub>	58.6	57.0	47.8	47.9	54.4	54.0	54.8
TiO <sub>2</sub>	0.99	1.01	0.60	0.57	0.79	0.40	0.41
Al <sub>2</sub> O <sub>3</sub>	14.6	14.2	8.9	8.0	11.1	11.8	12.8
Cr <sub>2</sub> O <sub>3</sub>	0.19	0.22	0.70	0.70	0.74	0.69	0.63
FeO	3.2	3.4	15.9	15.9	7.05	7.08	6.60
MgO	2.8	2.6	13.5	14.5	9.19	9.22	8.61
MnO	0.23	0.21	0.70	0.34	0.33	0.37	0.36
CaO	16.3	15.8	10.0	9.0	12.4	13.2	12.4
K <sub>2</sub> O	0.04	0.03	0.03	0.02	0.02	0.04	0.03
Na <sub>2</sub> O	3.1	3.1	1.9	1.75	2.43	2.05	2.52
P <sub>2</sub> O <sub>5</sub>	na	2.4	na	1.33	1.58	1.11	0.86
Total	100	100	100	100	100	100	100
equil. Fo	83.9	81.8	83.5	83.1	87.6	87.6	87.6
Si/Al <sup>f</sup>			3.6	4.0	3.2	3.1	2.9
Ca/Al/Cl			1.4	1.4	1.4	1.4	1.3

<sup>a</sup> Goodrich et al. (2001).

<sup>b</sup> 46 mol % added olivine (see text), adjusted for equilibrium with Fo  $\sim 83$  using  $\text{KD}_{\text{Fe/Mg}}(\text{ol/liq}) = 0.33$ .

<sup>c</sup> OIPTL evolved to near augite-saturation, then reduced to Fo 87.6 (see text).

<sup>d</sup> See text for derivation.

<sup>e</sup> See text for derivation.

<sup>f</sup> Molar ratio.

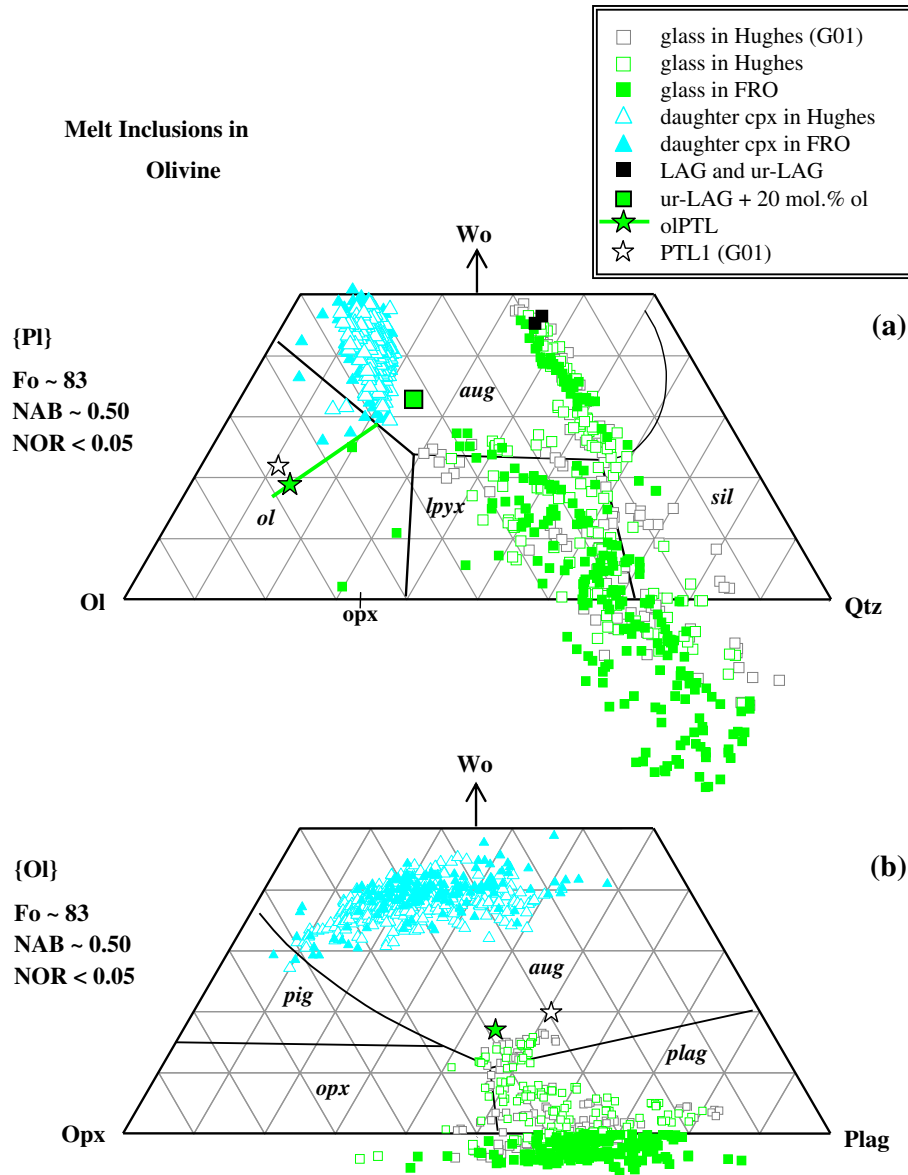


Fig. 7. Compositions of glass, daughter pyroxene (cpx) and reconstructed primary trapped liquid (PTL) compositions for melt inclusions in olivine in the phase systems (a) Olivine–Quartz–Wollastonite (Ol–Qtz–Wo) projected from plagioclase {Pl} and (b) Orthopyroxene–Plagioclase–Wollastonite (Opx–Plag–Wo) projected from olivine {Ol}. LAG = least aluminous glass and ur-LAG = extrapolation of LAG to inferred composition of trapped melt before crystallization of cpx (Goodrich et al., 2001). Ur-LAG and major glass trend are offset relative to trend expected from crystallization of daughter cpx (a). This offset can be explained by crystallization of ~20 mol % “excess” olivine as a result of reequilibration within the inclusions. Solid green line represents constraints on olivine component of the primary trapped liquid represented by melt inclusions in olivine (olTL). Example olPTL shown by green star has same olivine component as PTL1 of Goodrich et al. (2001). Phase boundaries from MAGPOX (Longhi, 1991) for melt in equilibrium with Fo 83 and alkali contents (NAB = normative albite; NOR = normative orthoclase) of olPTL (Table 5). G01 = Goodrich et al. (2001). See Longhi (1991) for projection equations.

dent of MgO) is what led to our mistaken addition of 10 mol % FeO to the ur-LAG to eliminate the offset in the glass trend in Ol–Qtz–Wo (Fig. 7a). With a correct understanding of the reequilibration process, however, we now recognize that this offset can also be eliminated by addition of ~20 mol % olivine (Fig. 7a), corresponding to the “excess” olivine described above. We note, however, that this is independent of the composition of the olivine, which means that we do not have any information about

the Fe/Mg ratio of the liquid before reequilibration and thus cannot use reverse fractionation crystallization to calculate the total amount of wall olivine. The requirement that the melt be olivine-saturated provides a minimum constraint of ~25–27 mol %. An estimate from the size of olivine halos (Goodrich et al., 2001) provides a maximum of ~50 mol %. This range of possible olPTL is shown in the Ol–Qtz–Wo and Opx–Plag–Wo systems in Fig. 7a and b. We emphasize that it is very likely that this melt was satu-

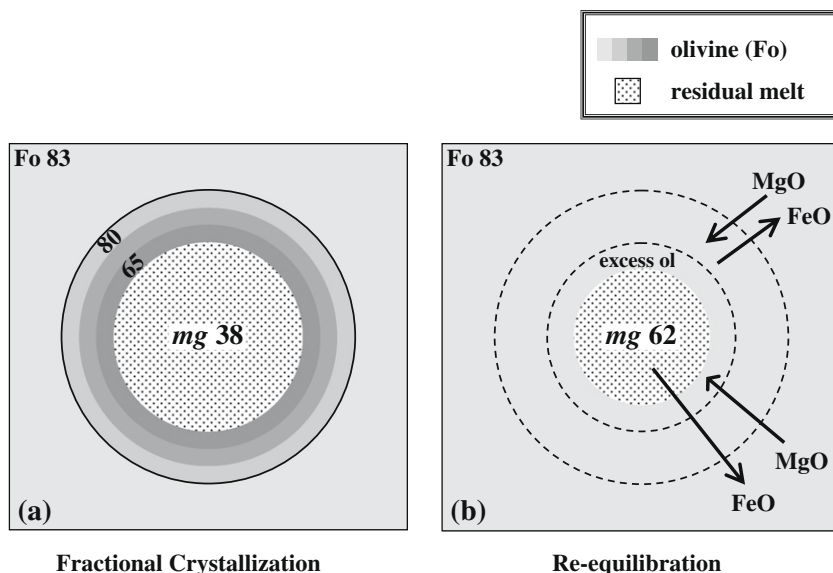


Fig. 8. Schematic illustration of (a) fractional crystallization and (b) re-equilibration of olivine-hosted melt inclusion with no daughter crystals. During re-equilibration, the fractionally crystallized wall olivine loses FeO and gains MgO from the surrounding host. The residual liquid in the inclusion likewise loses FeO and gains MgO, in order to maintain equilibrium with the olivine. However, the influx of MgO into the liquid causes it to become supersaturated with olivine, leading to crystallization of excess olivine relative to the case of no re-equilibration.

rated only with olivine, considering the high olivine content of the rocks.

The final step in reconstructing the composition of the PTL is to adjust Fe/Mg for equilibrium with olivine of the primary composition (i.e. at the time of entrapment). In the simplest case, as in most volcanic rocks, this would be the composition of the host (here  $Fo \sim 87$ ). However, in slowly cooled cumulates the primary olivine composition may not be preserved (e.g. Treiman, 1993). As discussed by Goodrich et al. (2001), the composition of olivine calculated to be in equilibrium with the primary pyroxenes at their QUILF (Andersen et al., 1993) equilibration temperature of  $1250 \pm 38^\circ\text{C}$  is  $Fo 83 \pm 1$ . This is also the composition with which the mean glass in the inclusions ( $mg 62$ ) would have been in equilibrium ( $KD_{Fe/Mg}(\text{ol/liq}) = 0.33$ ). Therefore, it appears that the inclusions equilibrated at high temperature with primary host olivine of  $Fo \sim 83$ . Taking this to be the case, we have calculated, as one example, an olPTL composition that has the same olivine component as olPTL1 of Goodrich et al. (2001) and thus can be directly compared to it (Table 5 and Fig. 7). The significant difference between the two is that the new olPTL has higher Si/Al ratio.

#### 4.2. Melt inclusions in augite

From petrographic observations we infer that melts trapped in augite crystallized augite onto their walls and then solidified the rest of the way as glass. The restricted range of compositions of the glasses (with the exception of those from section FRO 90054,07) suggests that they all crystallized approximately the same amount of wall augite. Rare metallic spherules in the inclusions do not appear to be products of a closed-system reaction as in the inclusions in olivine (Goodrich et al., 2001) because no chromite

is observed, and so were probably present in the primary melt. The composition of the PTL represented by these inclusions (augPTL) can thus be obtained by reintegrating wall augite with the average glass, and making necessary corrections for re-equilibration with the host.

The anomalous compositions of glasses and halo augite in the inclusions in FRO 90054,07 compared to those in other sections (Table 3) cannot be due to any observed differences in petrographic features. Although we cannot explain these values, their restriction to one section only suggests that they are due to contamination during sample preparation. Therefore, in calculating the average glass composition to be used in reconstruction of augPTL (Table 3), we exclude these analyses.

Although the observed variations in CaO and  $\text{Cr}_2\text{O}_3$  content of the surrounding augite are indicative of fractional crystallization, the spatial extent of zonation could not be documented adequately to constrain the amount of wall augite. A minimum value can be obtained from the assumption of augite saturation (i.e. location on the aug-plag boundary in Fig. 10b). We calculate this, by addition of augite of the primary FRO composition (Table 1) to be  $\sim 50$  mol %. However, given the absence of plagioclase in both the primary phase assemblage and the inclusions, it is likely that this value is too low. In principle, the correct value (and the composition of augPTL) can be obtained from a reverse fractional crystallization calculation (Sobolev and Shimizu, 1993) if the glass has not equilibrated Fe/Mg with its host. In fact, Fe/Mg ratios of the glasses in augite show considerable variation (Fig. 3) and range to higher values than would be in equilibrium with the primary augite. Thus, they may retain a record of their fractional crystallization history. If this is the case, the analysis with the highest Fe/Mg ratio ( $2.7 \pm 0.4$ ) represents the least degree of re-equilibration. Based on this assumption,

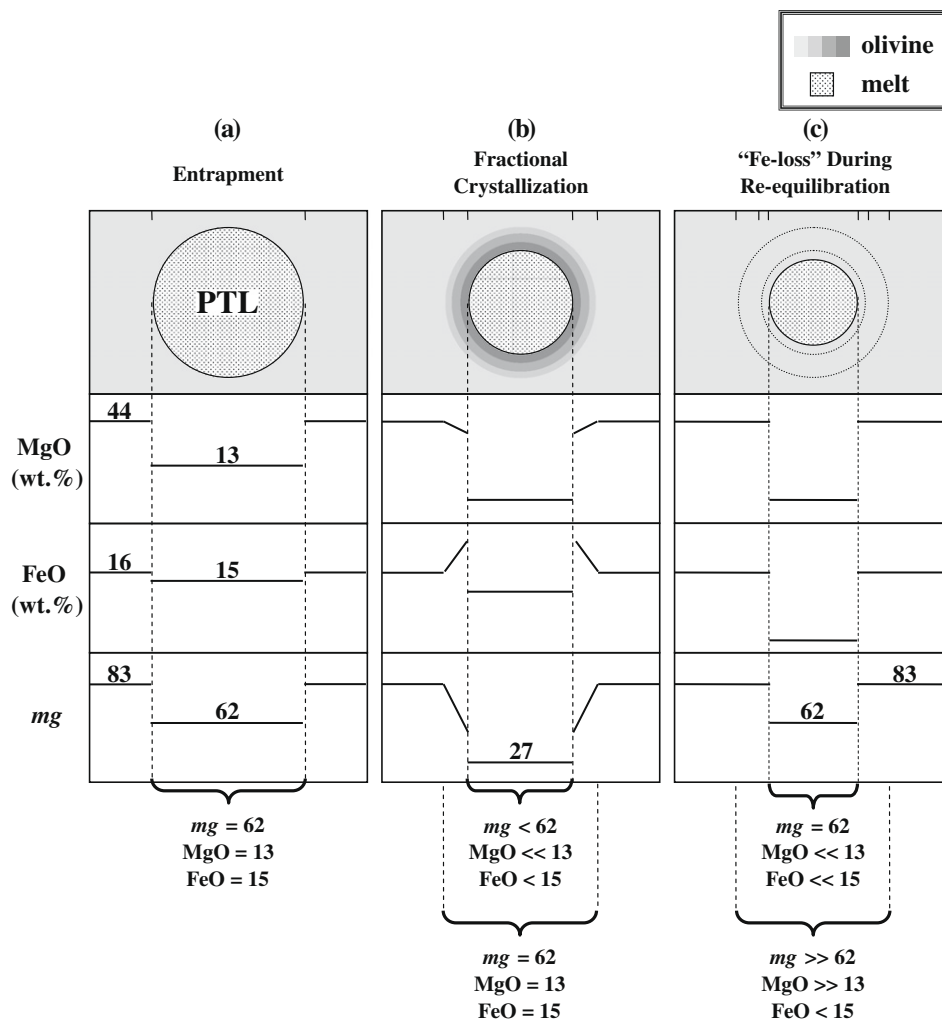


Fig. 9. Schematic illustration of reequilibration of olivine-hosted melt inclusion with no daughter crystals, showing changes in MgO and FeO as well as  $mg$ . (a) At time of entrapment, melt is in equilibrium with Fo 83 and has the same MgO, FeO and  $mg$  as the external body of magma. (b) Fractional crystallization of wall olivine greatly reduces MgO, and also reduces FeO and  $mg$  in the residual trapped melt, but the bulk composition of the original volume of the inclusion does not change. (c) During reequilibration with the host, the influx of MgO into the melt results in excess crystallization of olivine relative to the case of no reequilibration. Thus, MgO in the liquid remains constant while FeO decreases drastically. This effect is referred to as “Fe-loss” by Danyushevsky et al. (2000). The final melt (which is greatly reduced in volume but is now the only visible part of the inclusion) is in equilibrium with its host and has the same  $mg$  as the original trapped melt. However, its MgO and particularly FeO contents are greatly reduced relative to their values in the original trapped melt. Furthermore, the bulk composition of the original volume of the inclusion differs greatly from that of the primary trapped liquid (PTL).

we assign the average glass composition to have FeO and MgO values corresponding to the upper limit of this analysis (Table 3), and add wall augite by reverse fractional crystallization until the Fe/Mg composition of the primary augite ( $mg$  89.9) is reached.

The principle uncertainty involved in the calculation is the choice of  $KD_{Fe/Mg}$  (aug/liq), which shows much more variation than  $KD_{Fe/Mg}$  (oliv/liq). Experimental data suggest that it is positively correlated with  $mg$ , but uncertainties in the regression parameters are extremely high (Longhi and Pan, 1989; Longhi, 2003). Therefore, we take an empirical approach. For example, if we assume the composition of the primary augite in FRO ( $mg$  88.8) and the inferred composition of the primary olivine (Fo 83), then using  $KD_{Fe/Mg}$  (oliv/liq) = 0.33 (a typical value that gives

results consistent with QUILF) leads to  $KD_{Fe/Mg}$  (aug/liq) = 0.20. If instead we assume the present composition of olivine (Fo 87.6), this calculation yields  $KD_{Fe/Mg}$  (aug/liq) = 0.293. Using the former in the reverse fractional crystallization calculation gives the result that the primary augite composition is reached with addition of ~35 mol % wall augite. This value is lower than the minimum (~50 mol %) required to achieve augite saturation, and thus cannot be correct. In contrast, using  $KD_{Fe/Mg}$  (aug/liq) = 0.293 gives the result that the primary augite composition is reached with addition of ~81 mol % wall augite, and produces an augite-saturated PTL. This result suggests that at the point in the crystallization sequence at which melt was trapped in augite, the equilibrium olivine composition was similar to the present observed value.

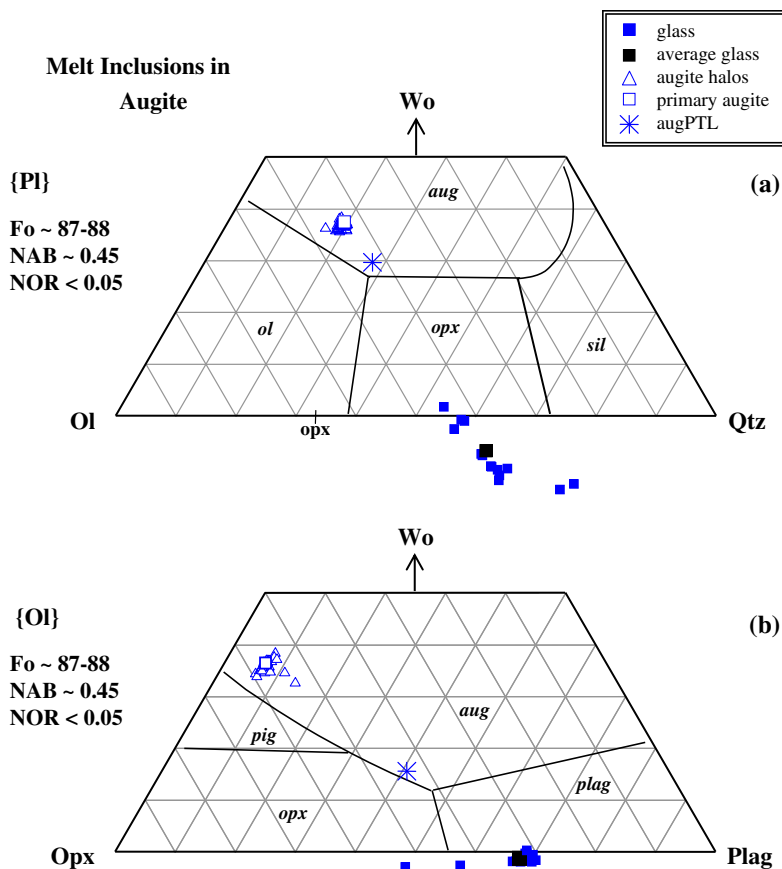


Fig. 10. Compositions of glass, halo augite and reconstructed composition of primary trapped liquid represented by melt inclusions in augite (augPTL) in the phase systems (a) Ol-Qtz-Wo and (b) Opx-Plag-Wo. Phase boundaries from MAGPOX (Longhi, 1991) for melt in equilibrium with Fo 87 and alkali contents of augPTL (Table 5).

The composition obtained from this calculation (augPTL) is given in Table 5 and shown in the Ol-Qtz-Wo and Opx-Plag-Wo systems in Fig. 10. We note that although the value obtained for the amount of wall augite greatly exceeds that expected from equilibrium crystallization, it is not extraordinary for melt inclusions in which heterogeneous nucleation of the host phase commonly causes it to overcrystallize (Frezzotti, 2001).

#### 4.3. Melt inclusions in orthopyroxene

From petrographic observations it can be inferred that after crystallization of wall orthopyroxene, melts trapped in orthopyroxene crystallized daughter cpx and then solidified the rest of the way as glass (again, metallic spherules appear to have been trapped along with the silicate melt, rather than derived from it by reduction). Thus, the composition of the primary trapped liquid (opxPTL) can be obtained by reversing the effects of crystallization of the daughter cpx, reintegrating the wall orthopyroxene, and making necessary corrections for Fe/Mg reequilibration with the host. The daughter cpx shows fractional crystallization trends similar those of daughter cpx in inclusions in olivine (Fig. 3). The glasses, however, show a restricted range of compositions suggesting that they all crystallized

approximately the same amount of cpx, and so there is no equivalent of the LAG. Therefore, we must reintegrate the glass and daughter cpx using modal recombination.

Point counting of the seven largest inclusions yielded 30–50 vol % cpx, which would correspond to ~35–60 wt% (assuming densities of ~3.3 and 2.7 g/cc for the cpx and the glass, respectively). Although the dataset is small, the restricted range of compositions (i.e. Al<sub>2</sub>O<sub>3</sub> content) of the glasses suggests that this result probably applies to all inclusions. The average composition of analyzed daughter cpx in the inclusions (Table 4) is similar to the composition of the primary augite, except for slightly lower CaO and higher Al<sub>2</sub>O<sub>3</sub>. In our calculations we take these two compositions as endmembers.

In considering the composition of glass to use in these calculations, we recognize that the glasses in orthopyroxene show significantly greater scatter than those in augite (Fig. 11), principally due to variations in SiO<sub>2</sub>/Na<sub>2</sub>O ratio associated with the spike in Na<sub>2</sub>O around 22 wt% Al<sub>2</sub>O<sub>3</sub> (Figs. 3 and 4). The reason for this spike is unclear. We do not believe it can be attributed to analytical problems, because of the care we took to eliminate Na mobility. One possible explanation is the unrecognized presence of small, heterogeneously-distributed plagioclase grains or nucleation centers in the glass. We note, however, that in

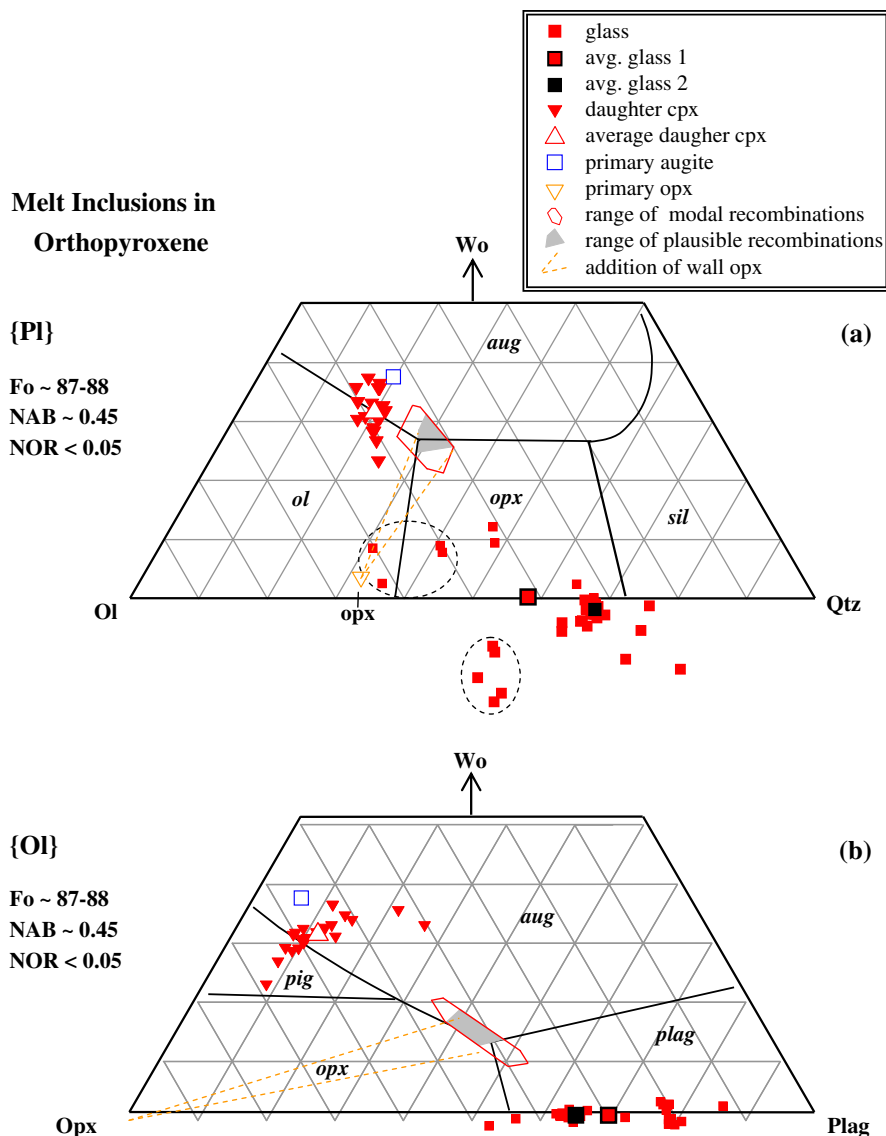


Fig. 11. Compositions of glass, daughter cpx and reconstructed composition of primary trapped liquid represented by melt inclusions in orthopyroxene (opxPTL) in the phase systems (a) Ol–Qtz–Wo and (b) Opx–Plag–Wo. Circled glass compositions are excluded from average glass 2 (Table 4). Phase boundaries from MAGPOX (Longhi, 1991) for melt in equilibrium with Fo 87 and alkali contents of opxPTL (Table 5).

the plagioclase projection (Fig. 11a), 8 out of the 10 inclusions analyzed show a well-defined trend with little scatter, while the other two (encircled) deviate to significantly lower  $\text{SiO}_2/\text{Na}_2\text{O}$  ratio. A strict average of all glass analyses is overly influenced by these inclusions because a larger number of analyses was obtained from them compared to some of the others. Because of these uncertainties, we chose to utilize two possible “averages” for the glass as endmembers in our calculation (Table 4): average glass 1 is the strict average of all analyses, while average glass 2 eliminates the two outlying inclusions and is thus the average for the main trend observed in the plagioclase projection (Fig. 11a).

Fe/Mg ratios in the inclusions suggest incomplete reequilibration. The glasses show significant variation in

Fe/Mg (Fig. 3) ranging to much higher values than would be in equilibrium with the host, and thus may retain a record of their fractional crystallization history. In contrast, the daughter cpx is reequilibrated (Table 4) and approximately in equilibrium with the least ferroan glass. Thus, the composition obtained by adding the daughter cpx in modal proportions to even the most ferroan glass would have an  $mg$  value that would not correspond to the state of the inclusion just after fractional crystallization of wall orthopyroxene and could not be used to obtain the amount of wall orthopyroxene by reverse fractional crystallization. In principle, however, we could start with the most ferroan glass (i.e. the average glass assigned the FeO and MgO of the most ferroan) and calculate reverse fractional crystallization of ~35–60 wt% daughter cpx, followed by orthopy-

roxene until the present primary Fe/Mg composition is reached. Regardless of which glass average or pyroxene is used, this calculation (using the same KD as above) produces the somewhat surprising result that primary olivine and pyroxene compositions are reached after reverse fractionation of ~40 wt% cpx, implying that there is essentially no wall orthopyroxene. One possible interpretation of this result is that even the most ferroan glass has partially reequilibrated and its Fe/Mg ratio is only a lower limit. On the other hand, it could be taken literally to show that the amount of wall orthopyroxene in these inclusions is extremely small. Although this result may be surprising, given the commonly observed tendency for the wall phase in a melt inclusion to overcrystallize (Frezzotti, 2001), it is a conclusion we also arrive at below for independent reasons.

A second approach we take is to reconstruct a range of compositions by combining each of the two endmember pyroxenes with each of the two glass averages in the ob-

served range of modal proportions. We then use MAGPOX (Longhi, 1991) calculations to evaluate which of these, after addition of wall orthopyroxene and adjustment of Fe/Mg for equilibrium with present compositions, is orthopyroxene-saturated. The full range of modal recombinations is shown in Fig. 11 outlined in red.

Of these, compositions formed dominantly from the average daughter cpx and average glass 1, have only olivine (or olivine plus plagioclase) on the liquidus, and do not become orthopyroxene-saturated even with addition of wall orthopyroxene. Thus, we eliminate them from consideration. Further, all compositions with less than ~40 wt% cpx have plagioclase ( $\pm$ olivine) on the liquidus. Although these may become plagioclase + orthopyroxene-saturated with addition of wall orthopyroxene (Fig. 11b), they are unlikely compositions for opxPTL because no plagioclase is observed in the inclusions. Thus, we eliminate these as well. Of the remaining compositions, those with more than

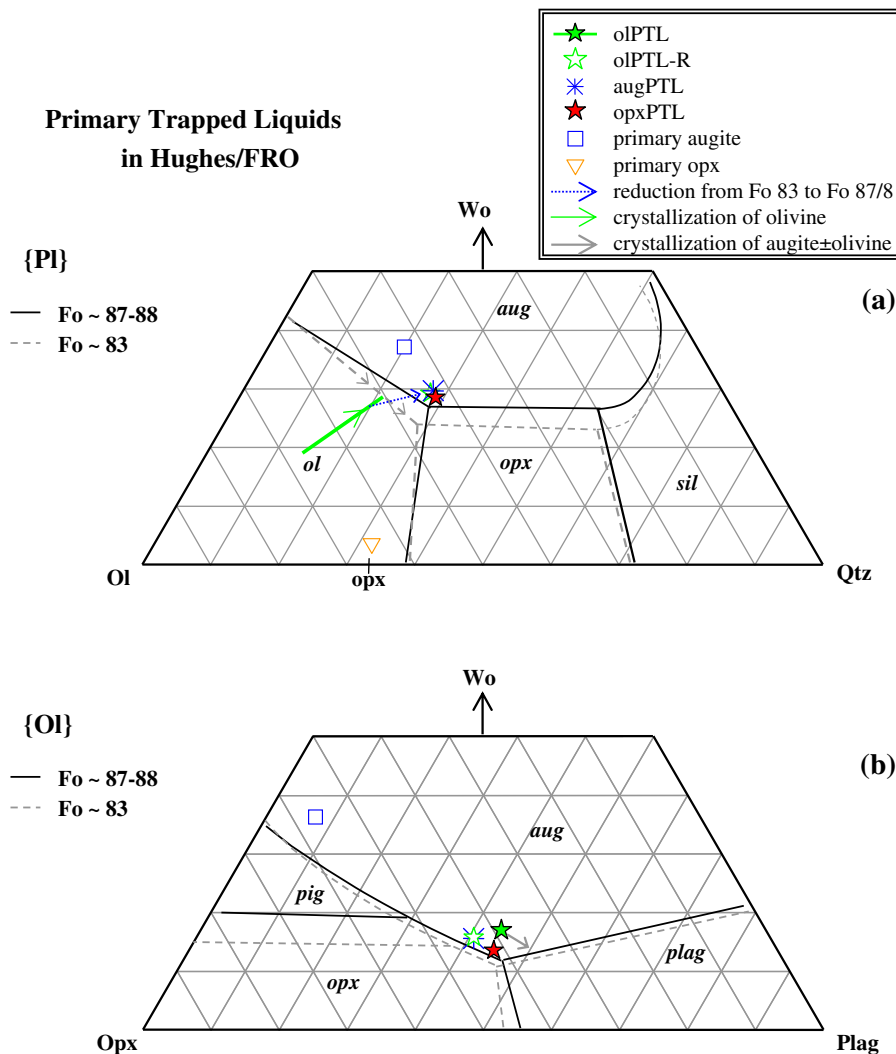


Fig. 12. (a) Oliv–Qtz–Wo and (b) Opx–Plag–Wo systems showing reconstructed compositions of primary trapped liquids represented by melt inclusions in olivine (olPTL), augite (augPTL) and orthopyroxene (opxPTL). OIPTL does not evolve to augPTL or opxPTL in the course of normal magmatic evolution (crystallization of olivine followed by olivine + augite). However, it may do so if it is reduced from Fo 83 to Fo 87 before it reaches augite saturation.

~55 wt% cpx have only augite on the liquidus and become olivine- (rather than orthopyroxene-) saturated upon addition of wall orthopyroxene (Fig. 11a), and thus are also eliminated. The resulting field of plausible compositions is shown in grey in Fig. 11, and the effect of adding wall orthopyroxene to any of these is shown by the orange dashed lines.

#### 4.4. Magmatic evolution

The melt trapped in olivine in Hughes and FRO (olPTL) can be reasonably assumed to represent the parent magma of these rocks. As discussed above, there is evidence that olPTL was in equilibrium with olivine of ~Fo 83, rather than the present composition of Fo 87–8. Goodrich et al. (2001) suggested that this difference was due to subsolidus reequilibration. However, in this work we have shown that the melts trapped in augite and orthopyroxene were in equilibrium with olivine of Fo 87–8. Thus, it appears that the evolution of the Hughes/FRO magma followed a reverse (relative to the normal trend) fractionation trend. In the smelting model for ureilites, reverse magmatic evolution would be a natural consequence of ascent of a magma, since decreasing pressure results in reduction (Goodrich et al.,

2007). Therefore we suggest that crystallization of olPTL began during ascension, before it was emplaced at its final depth in the UPB. In this model, the majority of olivine crystals now present must have crystallized at a depth at which carbon redox reactions buffered a composition of Fo ~ 83 and been entrained in the rising magma. Crystallization of augite and orthopyroxene then occurred at a shallower location (near or at its final resting place) where the equilibrium Fo was 87–8, and earlier-formed olivine reequilibrated to this composition. We now demonstrate that the reconstructed PTL are consistent with this interpretation.

It can be seen in Fig. 12 that normal magmatic evolution of olPTL (crystallization of olivine followed by olivine + augite) does not lead to augPTL. However, if olPTL (assumed to be saturated only with olivine, as discussed above) is allowed to evolve by olivine crystallization to a point that is slightly short of augite-cosaturation, and then is reduced to Fo 87–8, it results in a composition (olPTL-R) that is very similar to augPTL (Fig. 12 and Table 5), and like augPTL is not saturated with olivine. Thus, the reduction model to explain the Fo 83 to Fo 87–8 evolution could also explain the petrologic evolution from olPTL to augPTL.

OIPTL-R and augPTL are initially saturated only with augite. However, after a few percent crystallization they become saturated with orthopyroxene and are within the range of plausible compositions for opxPTL (Fig. 11). We have identified a narrow range of these compositions that are very similar to augPTL (or can be related to it by a few percent crystallization of augite) and are orthopyroxene-saturated. One example is given in Table 5 and shown in Fig. 12. These compositions all contain ~40–45 wt% daughter cpx, and contain at most a few percent wall orthopyroxene. The latter requirement, in particular, severely restricts the mix. Addition of more than a few percent orthopyroxene results in compositions that cannot be related to augPTL by any combination of augite crystallization or reduction. Thus, if we assume that opxPTL is related to olPTL-R and augPTL by closed-system evolution we arrive at the same conclusion as above, namely, that these melt inclusions crystallized only a very small amount of the wall phase. This would be consistent with the lack of minor element zonation around the inclusions, and not unreasonable if opxPTL was just barely orthopyroxene-saturated. Furthermore, overcrystallization of the wall phase would not necessarily have been favored in this case, because the second phase to saturate was also a pyroxene (the expectation of overcrystallization of the wall phase derives from cases in which the second phase to saturate is structurally very different from the host, e.g. pyroxene in inclusions in olivine). These arguments, therefore, strongly suggest that augPTL and opxPTL were very similar, and were trapped in their hosts at approximately the same time. The implication that augite and orthopyroxene co-crystallized in Hughes and FRO in an important conclusion, because it could explain the absence of augite–orthopyroxene–augite reaction textures observed in other augite-bearing ureilites (Goodrich, 1999a; Goodrich and Keller, 2000; Berkley and Goodrich, 2001).

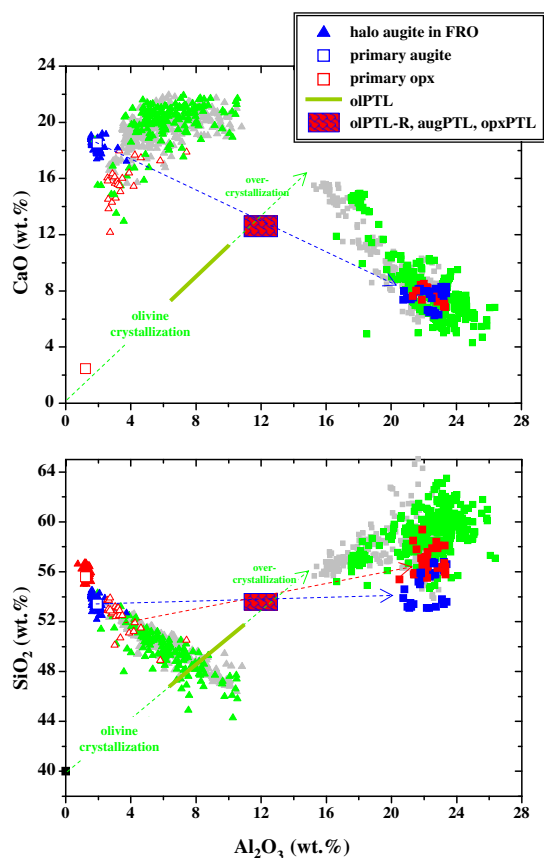


Fig. 13.  $\text{Al}_2\text{O}_3$  vs.  $\text{CaO}$  and  $\text{SiO}_2$  (all wt%) for all primary phases and melt inclusions in Hughes and FRO, illustrating difference between crystallization path of magma within the inclusions compared to the external body of magma. Symbols not identified in legend are same as in Fig. 3.

Table 6  
Crystal/liquid distribution coefficients for REE.

	Primary silicates			Inclusions in olivine augite <sup>d</sup>
	Augite <sup>a</sup>	Opx <sup>b</sup>	Olivine <sup>c</sup>	
La	0.0366	0.00087		0.059
Ce	0.0577	0.00141		0.086
Nd	0.1317	0.00501	0.00007	0.167
Sm	0.2054	0.01424	0.00058	0.252
Eu (IW-2) <sup>e</sup>	0.1			
Eu (IW-3) <sup>f</sup>				0.052
Gd			0.00102	0.283
Dy		0.05582		
Yb	0.3019	0.15115	0.01940	0.316
Lu	0.3102	0.17701		0.325

<sup>a</sup> Calculated for Wo 37 from McKay et al. (1986), except Eu. Eu extrapolated to  $fO_2 = IW-2$  from Grutzeck et al. (1974).

<sup>b</sup> Values for low-Ca pyroxene of Wo 5 (McKay et al., 1991).

<sup>c</sup> Values for mare basalt-like compositions (McKay, 1986).

<sup>d</sup> Calculated for Wo 42 from McKay et al. (1986), except Eu. Eu extrapolated to  $fO_2 = IW-3$  from Grutzeck et al. (1974).

<sup>e</sup> Inferred primary  $fO_2$  based on C redox equilibria.

<sup>f</sup> Inferred late  $fO_2$  within inclusions, based on C redox equilibria.

One possible challenge to this model is the unusual inclusion #24 in olivine (Fig. 2e). The interpretation that the orthopyroxene grain in this inclusion is cognate (Fioretti and Goodrich, 2000) would imply that at least some olivine was crystallizing at the same time as orthopyroxene, which is inconsistent with our conclusion that olPTL-R, augPTL and opxPTL were not olivine-saturated. An alternative possibility, suggested by the unusually high degree of secondary reduction of this inclusion, is that in this rare case the melt trapped in an early olivine crystal was strongly reduced before a significant amount of wall olivine crystallized, which could have the effect of driving it into the field of orthopyroxene stability. Crystallization of orthopyroxene would then drive it back toward augite, which could explain the textural evidence for reaction of orthopyroxene to form augite.

As an additional check on whether the derived PTLs are reasonable, we can also compare the crystallization sequences within the melt inclusions to that of the external body of magma. Restricting this analysis to major elements (other than FeO and MgO), Fig. 13 shows that in terms of both CaO–Al<sub>2</sub>O<sub>3</sub> and SiO<sub>2</sub>–Al<sub>2</sub>O<sub>3</sub> trends, crystallization of olivine alone leads olPTL directly to the composition(s) of olPTL-R, augPTL and opxPTL. From this point, overcrystallization of olivine within the inclusions in olivine leads to the beginning of the observed glass trend for the inclusions in olivine (after which the trend is determined by fractional crystallization of daughter cpx, as demonstrated by Goodrich et al. (2001)). In contrast, in the inclusions in augite and orthopyroxene there is no crystallization of olivine, and crystallization of only augite (halo augite for inclusions in augite and daughter cpx for inclusions in orthopyroxene) leads directly to the compositions of residual glasses.

#### 4.5. Rare earth elements in the Hughes/FRO parent magma

We have calculated REE abundances for liquids in equilibrium with the primary olivine, augite and orthopyroxene in Hughes/FRO, using the average of measured REE abun-

dances for each phase and crystal/liquid distribution coefficients ( $D$ ) appropriate for primary mineral compositions (parameterized in terms of Wo for the pyroxenes) and  $fO_2$  (Table 6). In addition, under the assumption that the low-Al<sub>2</sub>O<sub>3</sub> glass in melt inclusions in olivine represents the composition of the trapped liquid after crystallization only of wall olivine (~40 wt%), we have calculated REE abundances for olPTL. These four calculations give very similar results (Fig. 6e), and thus provide a well-constrained REE composition for the Hughes/FRO parent magma. This composition is strongly LREE-depleted (CI-normalized Sm/La ~ 3.3–3.7) with a small negative Eu anomaly (Eu/Eu\* ~ 0.82), and shows a slight HREE-depletion as well (CI-normalized Gd/Lu ~ 1.4–1.6).

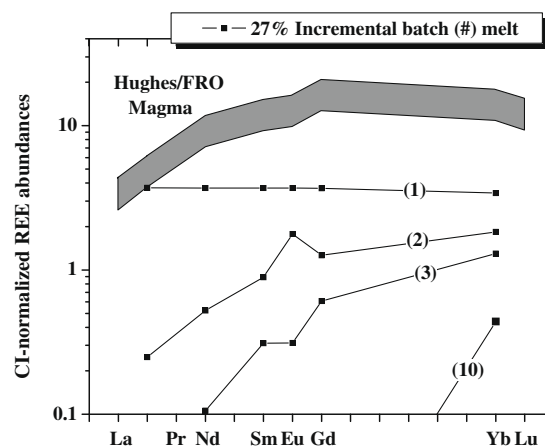


Fig. 14. CI-normalized rare earth element (REE) abundances in the Hughes/FRO parent magma (from Fig. 6e and allowing for possible prior crystallization of 40 wt% olivine), compared to calculated REE abundances in 27% partial melt (saturated only with olivine) of CV-like source with Ca/Al ~ 1.4 × CI (Goodrich, 1999b). Results shown are for 1, 2, 3 and 10 batches of melt extraction using the incremental batch melting model of Allegre and Minster (1978). CI abundances from Anders and Ebihara (1982).

REE abundances of daughter cpx and the higher-Al<sub>2</sub>O<sub>3</sub> glasses in the inclusions in olivine, however, may reflect closed-system crystallization and/or reequilibration processes. For example, although the observed correlation between LREE abundances and Al<sub>2</sub>O<sub>3</sub> content of glasses (Fig. 6d) suggests that their REE patterns reflect fractional crystallization and have not been modified by reequilibration, this is not borne out quantitatively. Calculation of REE abundances for a liquid in equilibrium with the average daughter cpx in the inclusions, using *D* values again parameterized in terms of *Wo* and *f*O<sub>2</sub> in the inclusions (Table 6), yields a pattern that is similar to that of the high-Al<sub>2</sub>O<sub>3</sub> glasses but at an absolute level ~2–2.5 × higher (Fig. 6f). A similar result is obtained by calculation of 30–50% fractional crystallization of augite from the low-Al<sub>2</sub>O<sub>3</sub> glass (Fig. 6f). This discrepancy cannot be explained by crystallization of wall olivine, because that effect is already recorded in the low-Al<sub>2</sub>O<sub>3</sub> glass. It may be partly explained by the very high Al<sub>2</sub>O<sub>3</sub> contents (up to 11 wt%) and *mg* of the daughter cpx. In combination, these two compositional parameters lead to higher REE *D* values (McKay et al., 1988; Wood and Blundy, 1997), which would result in a better fit. However, the extreme degree of fractionation recorded in the pyroxenes also suggests the possibility that equilibrium was not completely attained.

#### 4.6. Source of the Hughes/FRO parent magma on the UPB

We have obtained a composition for the parent magma of Hughes and FRO that is well constrained in terms of most major and minor elements, as well as REE, and which is consistent with crystallization in an environment in which *f*O<sub>2</sub> (thus *mg* of silicates) was controlled by pressure-dependent carbon redox reactions. This magma composition can be used to evaluate models for the petrogenesis of augite-bearing ureilites.

The main problem presented by the augite-bearing ureilites is that melts that crystallize in the sequence olivine → augite → orthopyroxene cannot be simply related to olivine-lpx residues (i.e. the majority of ureilites). Such melts can only be derived from starting compositions that plot to the right of the augite-lpx phase boundary in the system Opx–Plag–Wo (Fig. 12b), while olivine-lpx residues can only be derived from starting compositions that plot to the left of it. In the context of a smelting model, however, the former might simply be deeper versions of the latter, since progressive reduction (i.e. loss of FeO) can move a composition from the augite to the pigeonite to the orthopyroxene stability field. Based on this observation, Goodrich et al. (2004, 2006) suggested that the parent magmas of the augite-bearing ureilites were generated in deeper, more ferroan source regions than those represented by the olivine-lpx ureilites, and then were reduced during ascent and/or emplacement at shallower levels. The evidence presented here for reduction of the Hughes/FRO parent magma from Fo 83 to Fo 87 during crystallization supports such a model.

However, for several reasons, the composition of the Hughes/FRO parent magma does not appear to be consistent with derivation as a primary melt on the UPB. First of

all, it is clearly not consistent with direct derivation from source materials having the high Ca/Al ratios (2–2.5 × CI) that are required to produce the olivine-lpx ureilites (Goodrich, 1999b; Goodrich et al., 2007), because if it was saturated only with olivine its Ca/Al ratio (~1.4 × CI) must be essentially the same as that of its source (Fig. 12b). At the same time, calculation of the expected REE patterns of high-degree melts of such a source (similar to CC-like compositions examined in Goodrich (1999b)) show much lower abundances than the Hughes/FRO magma, even allowing for possible prior crystallization of olivine (Fig. 14). Other aspects of its composition, such as relatively high Na<sub>2</sub>O and P<sub>2</sub>O<sub>5</sub> contents, also seem to be inconsistent with a high-degree melt.

These observations suggest an alternative type of model, namely that the parent magmas of augite-bearing ureilites are not primary melts, but rather products of mixing and/or assimilation. Mixing/assimilation models are, in fact, strongly suggested by the complex reaction textures observed in most of the augite-bearing ureilites (e.g. Berkley and Goodrich, 2001), and would be consistent with the suggestion (Goodrich et al., 2004, 2006) that magmas derived from deep source regions ascended and were emplaced within the column of olivine-lpx ureilite residues. Although examination of such models is beyond the scope of this paper, the composition derived here for the Hughes/FRO parent magma provides a robust constraint for future work along these lines.

#### ACKNOWLEDGMENTS

We thank John Longhi, Leonid Danyushevsky, Harold Connolly, David Mittlefehldt, Allan Treiman, Tim Grove, Michael Weisberg and Lionel Wilson for helpful discussions. We thank Elvira Macsenaere-Riester and Burkhard Schulz-Dobrick for assistance with EMPA, and Peter Hoppe, Elmar Gröner, Roger Strebel and Jutta Zipfel for assistance with SIMS. We are grateful to Luigi Folco (Museo Nazionale per l'Antartide) and Caroline Smith (Natural History Museum) for the loan of thin sections of FRO meteorites. We thank reviewers Alex Ruzicka, John Longhi, and the associate editor Christian Koeberl, for reviews that led to significant improvement of this manuscript. This work was supported by Max-Planck Institut für Chemie, NASA Grant NNG05GH72G to C.A. Goodrich, NASA Grant NNX08AG63G to C.A. Goodrich (P.I.) and J.A. Van Orman (Co-I), NSF Grant 0337125 to J.A. Van Orman, and a grant ("Antarctic Meteorites") from Programma Nazionale di Ricerche in Antartide (PNRA) to A.M. Fioretti.

#### APPENDIX A. SUPPLEMENTARY DATA

Supplementary data associated with this article can be found, in the online version, at [doi:10.1016/j.gca.2009.02.018](https://doi.org/10.1016/j.gca.2009.02.018).

#### REFERENCES

- Allegre C. J. and Minster J. F. (1978) Quantitative models of trace element behavior in magmatic processes. *Earth Planet. Sci. Lett.* **38**, 1–25.
- Anders E. and Ebihara M. (1982) Solar system abundances of the elements. *Geochim. Cosmochim. Acta* **46**, 2363–2380.

- Andersen D. J., Lindsley D. H. and Davidson P. M. (1993) QUILF: a PASCAL program to assess equilibria among Fe–Mg–Mn–Ti oxides, pyroxenes, olivine, and quartz. *Comput. Geosci.* **19**, 1333–1350.
- Baba T., Takeda H. and Saiki K. (1993) Mineralogy of three Euromet ureilites including an orthopyroxene–augite achondrite. *Meteoritics* **28**, 319 (abstr.).
- Berkley J. L. and Goodrich C. A. (2001) Evidence for multi-episodic igneous events in ureilite MET 78008. *Meteorit. Planet. Sci.* **36**, A18–A19 (abstr.).
- Berkley J. L. and Jones J. H. (1982) Primary igneous carbon in ureilites: petrological implications. *Proc. Lunar Planet. Sci. Conf.* **13**, A353–A364.
- Danyushevsky L. V., Della-Pasqua F. N. and Sokolov S. (2000) Re-equilibration of melt inclusions trapped by magnesian olivine phenocrysts from subduction-related magmas: petrological implications. *Contrib. Mineral. Petrol.* **138**, 68–83.
- Danyushevsky L. V., Sokolov S. and Falloon T. J. (2002a) Melt inclusions in olivine phenocrysts: using diffusive re-equilibration to determine the cooling history of a crystal, with implications for the origin of olivine-phyric volcanic rocks. *J. Petrol.* **43**, 1651–1671.
- Danyushevsky L. V., McNeil A. W. and Sobolev A. V. (2002b) Experimental and petrological studies of melt inclusions in phenocrysts from mantle-derived magmas: an overview of techniques, advantages and complications. *Chem. Geol.* **183**, 5–24.
- Fioretti A. M. and Goodrich C. A. (2000) Primary melt inclusions in olivine, augite and orthopyroxene in ureilite FRO 90054. *Lunar Planet. Sci.* **31**, #1202 (abstr.).
- Fioretti A. M. and Goodrich C. A. (2001) A contact between an olivine–pigeonite lithology and an olivine–augite–orthopyroxene lithology in ureilite FRO 93008: dashed hopes? *Meteorit. Planet. Sci.* **36**, A58 (abstr.).
- Fioretti A. M. and Molin G. (1996) Petrography and mineralogy of FRO 93008 ureilite: evidence for pairing with FRO 90054 ureilite. *Meteorit. Planet. Sci. Suppl.* **31**, A43 (abstr.).
- Gaetani G. L. and Watson E. B. (2000) Open system behavior of olivine-hosted melt inclusions. *Earth Planet. Sci. Lett.* **183**, 27–41.
- Frezza M.-L. (2001) Silicate–melt inclusions in magmatic rocks: applications to petrology. *Lithos* **55**, 273–299.
- Goodrich C. A. (1992) Ureilites: a critical review. *Meteoritics* **27**, 327–352.
- Goodrich C. A. (1999a) A primary silicate mineral/melt reaction texture in ureilite LEW 88774. *Meteorit. Planet. Sci.* **34**, A44–A45 (abstr.).
- Goodrich C. A. (1999b) Are ureilites residues from partial melting of chondritic material? The answer from MAGPOX. *Meteorit. Planet. Sci.* **34**, 109–119.
- Goodrich C. A. (2001) Magmatic inclusions in Frontier Mountain 90054 and Elephant Moraine 96328: complex petrogenesis of the olivine–(augite)–orthopyroxene ureilites. *Lunar Planet. Sci.* **32**, 23, #1300 (abstr.).
- Goodrich C. A. and Delaney J. S. (2000) Fe/Mg–Fe/Mn relations of meteorites and primary heterogeneity of primitive achondrite parent bodies. *Geochim. Cosmochim. Acta* **64**, 2255–2273.
- Goodrich C. A. and Fioretti A. M. (2000) The parent magmas of ureilites FRO 90054 and Hughes 009: inferences from melt inclusions in FRO 90054. *Lunar Planet. Sci.* **31**, #1226.
- Goodrich C. A. and Fioretti A. M. (2007) The parent magma of ureilite Hughes 009 (re)inferred from melt inclusions in olivine: implications for petrogenesis of augite-bearing ureilites. *Lunar Planet. Sci.* **38**, 21, #1083 (abstr.).
- Goodrich C. A. and Keller L. P. (2000) Transmission electron microscope investigation of a silicate mineral/melt reaction texture in ureilite LEWIS CLIFF 88774. *Meteorit. Planet. Sci.* **35**, A60–A61 (abstr.).
- Goodrich C. A., Jones J. H. and Berkley J. L. (1987) Origin and evolution of the ureilite parent magmas: multi-stage igneous activity on a large parent body. *Geochim. Cosmochim. Acta* **51**, 2255–2273.
- Goodrich C. A., Fioretti A. M. and Hoppe P. (2000) Rare earth elements in primary melt inclusions in olivine in ureilite Hughes 009. *Lunar Planet. Sci.* **31**, #1192 (abstr.).
- Goodrich C. A., Fioretti A. M., Tribaudino M. and Molin G. (2001) Primary trapped melt inclusions in olivine in the olivine–augite–orthopyroxene ureilite Hughes 009. *Geochim. Cosmochim. Acta* **65**, 621–652.
- Goodrich C. A., Scott E. R. D. and Fioretti A. M. (2004) Ureilitic breccias: clues to the petrologic structure and impact disruption of the ureilite parent asteroid. *Chem. Erde* **64**, 283–327.
- Goodrich C. A., Wlotzka F., Ross D. K. and Bartoschewitz R. (2006) NWA 1500: plagioclase-bearing monomict ureilite or ungrouped achondrite? *Meteorit. Planet. Sci.* **41**, 925–952.
- Goodrich C. A., Van Orman J. and Wilson L. (2007) Fractional melting and smelting on the ureilite parent body. *Geochim. Cosmochim. Acta* **71**, 2876–2895.
- Grady M. M. and Pillinger C. T. (1993) EUROMET ureilite consortium: a preliminary report on carbon and nitrogen geochemistry. *Lunar Planet. Sci.* **24**, 551–552 (abstr.).
- Grutzeck M., Kridelbaugh S. and Weill D. (1974) The distribution of Sr and REE between diopside and silicate liquid. *Geophys. Res. Lett.* **1**, 273–275.
- Guan Y. and Crozaz G. (2000) Light rare earth element enrichments in ureilites: a detailed ion microprobe study. *Meteorit. Planet. Sci.* **35**, 131–144.
- Ikeda Y. (1998) Petrology of magmatic silicate inclusions in the Allan Hills 77005 lherzolitic shergottite. *Meteorit. Planet. Sci.* **33**, 803–812.
- Jochum K. P., Dingwell D. B., Hofmann A. W., Stoll B., Raczek I., Rocholl A., Becker S., Bismehn A., Bessette D., Dietze H.-J., Dulski P., Erzinger J., Hellebrand E., Hoppe P., Horn I., Janssens K., Jenner G., Klein M., McDonough W. M., Maetz M., Nikogosian I. K., Pickhardt C., Seufert H. M., Simakin S. G., Sobolev A. V., Spettel B., Straub S., Vincze L., Wallianos A., Weckwerth G., Wolf D. and Zimmer M. (2000) The preparation and preliminary characterization of eight geological MPI-DING reference glasses for in-situ microanalysis. *Geostand. Newslett.* **24**, 87–133.
- Longhi J. (1991) Comparative liquidus equilibria of hypersthene-normative basalts at low pressure. *Am. Mineral.* **76**, 785–800.
- Longhi J. (2003) A new view of lunar ferroan anorthosites: postmagma ocean petrogenesis. *J. Geophys. Res.* **108**, E8, 5083. doi: 10.1029/2002JE001941.
- Longhi J. and Pan V. (1989) The parent magmas of the SNC meteorites. *Proc. Lunar Planet. Sci. Conf.* **19**, 451–464.
- McKay G. A. (1986) Crystal/liquid partitioning of REE in basaltic systems: extreme fractionation of REE in olivine. *Geochim. Cosmochim. Acta* **50**, 69–79.
- McKay G., Wagstaff J. and Yang S.-R. (1986) Clinopyroxene REE distribution coefficients for shergottites: the REE content of the Shergotty melt. *Geochim. Cosmochim. Acta* **50**, 927–937.
- McKay G., Le L., Wagstaff J. and Lindstrom D. (1988) Experimental trace element partitioning for LEW86010: petrogenesis of a unique achondrite. *Meteoritics* **23**, 289 (abstr.).
- McKay G., Le L. and Wagstaff J. (1991) Constraints on the origin of the mare basalt europium anomaly: REE partition coefficients for pigeonite. *Lunar Planet. Sci.* **22**, 883–884 (abstr.).
- Mittlefehldt D. W., McCoy T. J., Goodrich C. A. and Kracher A. (1998) Non-chondritic meteorites from asteroidal bodies. In

- Planetary Materials*, vol. 36 (ed. J.J. Papike). Mineralogical Society of America. Rev. Mineral., 195 pp.
- Rocholl A. B. E., Simon K., Jochum K. P., Bruhn F., Gehann R., Kramar U., Luecke W., Molzahn M., Pernicka E., Seufert M., Spettel B. and Stummeier J. (1997) Chemical Characterization of NIST Silicate Glass Certified Reference Material SRM 610 by ICP-MS, TIMS, LIMS, SSMS, INAA, AAS and PIXE. *Geostand. Newslett.* **21**, 101–114.
- Roedder E. (1976) Petrologic data from experimental studies on crystallized silicate melt and other inclusions in lunar and Hawaiian olivine. *Am. Mineral.* **61**, 684–690.
- Roedder E. (1979) Origin and significance of magmatic inclusions. *Bull. Mineral.* **102**, 487–510.
- Singletary S. J. and Grove T. L. (2003) Early petrologic processes on the ureilite parent body. *Meteorit. Planet. Sci.* **38**, 95–108.
- Sinha S. K., Sack R. O. and Lipschutz M. E. (1997) Ureilite meteorites: equilibration temperatures and smelting reactions. *Geochim. Cosmochim. Acta* **61**, 4325–4342.
- Smith C. L., Franchi I. A., Wright I. P., Grady M. M., Verchovsky A. B. and Pillinger C. T. (1999) A preliminary noble gas and light element stable isotopic study of the FRO 90228 low-carbon ureilite. *Meteorit. Planet. Sci.* **34**, A110 (abstr.).
- Smith C. L., Wright I. P., Franchi I. A. and Grady M. M. (2000) A statistical analysis of mineralogical data from Frontier Mountain ureilites. *Meteorit. Planet. Sci.* **35**, A150 (abstr.).
- Sobolev A. V. (1996) Melt inclusions in minerals as a source of principle petrological information. *Petrology* **4**, 209–220. Translated from *Petrologiya* 4, 228–239.
- Sobolev A. V. and Shimizu N. (1993) Ultra-depleted primary melt included in an olivine from the Mid-Atlantic Ridge. *Nature* **363**, 151–154.
- Treiman A. (1993) The parent magma of the Nakhla (SNC) meteorite, inferred from magmatic inclusions. *Geochim. Cosmochim. Acta* **57**, 4753–4767.
- Tribaudino M., Fioretti A. M., Martignago F. and Molin G. (1997) Transmission electron microscope texture and crystal chemistry of coexisting ortho- and clinopyroxene in the Antarctic ureilite Frontier Mountain 90054: implications for thermal history. *Meteorit. Planet. Sci.* **32**, 671–678.
- Walker D. and Grove T. L. (1993) Ureilite smelting. *Meteoritics* **28**, 629–636.
- Warren P. H. and Kallemeyn G. W. (1992) Explosive volcanism and the graphite-oxygen fugacity buffer on the parent asteroid(s) of the ureilite meteorites. *Icarus* **100**, 110–126.
- Wilson L., Goodrich C. A. and Van Orman J. (2008) Thermal evolution and physics of melt extraction on the ureilite parent body. *Geochim. Cosmochim. Acta* **72**, 6154–6176.
- Wood B. J. and Blundy J. D. (1997) A predictive model for rare earth element partitioning between clinopyroxene and anhydrous silicate melt. *Contrib. Mineral. Petrol.* **129**, 166–181.
- Zinner E. and Crozaz G. (1986) A method for the quantitative measurement of rare earth elements in the ion microprobe. *Int. J. Mass. Spect. Ion Processes* **69**, 17–38.

Associate editor: Christian Koeberl